BRAIN AND COGNITION 21, 226–246 (1993)

Neuroelectric Concepts: Form–Color Classification

WILLIAM J. HUDSPETH

Neuropsychometrics Laboratory and Department of Psychology, Radford University

Visual event-related potentials (VEPs) were recorded from the scalp of human observers who viewed an orthogonal stimulus set, consisting of four stimuli, each of which had two attributes: a form (circle or triangle) and a color (green or red). The stimulus set was represented by an a priori stimulus classification model, defined by positions (i.e., degrees of arc) on a unit circle that specified the relationships among the form and color features. An analysis of VEP deviation waveshapes (ΔVEP: deviations around average VEP for each electrode) showed that the a priori unit circle model predicted morphologies of the ΔVEP waveshapes, as well as the overall relationships between waveshapes obtained for the form and the color attributes. Further analyses demonstrated that individual ΔVEP waveshapes for color and for form were located on the circumference of a unit circle at the positions (angle) specified by the a priori model. The studies show that formal modeling of the way humans classify stimulus attributes provides a quantitative and predictive model of the way VEPs become classified and organized according to psychological principles.

INTRODUCTION

Visual pattern recognition can be analyzed according to hierarchical (i.e., top–down) neural processes that organize concepts, percepts, and sensory images. The question to be addressed in this report is: When records of brain electrical activities are obtained during visual stimulation, do the obtained measurements reflect sensory imaging, perceptual constancies, or the conceptual classification of the stimuli presented to experimental subjects?

Scalp recordings of visual event-related potentials (VEPs) have been used to investigate a number of functions of the human visual system,

I thank Robert Thatcher for many challenging discussions while developing the quantitative model reported in this work. I am grateful to Karl Pribram and Lauren Gerbrandt for their interest, comments, and criticisms while preparing the manuscript. I also thank Ms. Amy Garrett for helping me develop the geometric algorithms and Ms. Candy Disch for preparing subjects in the experiments. Address reprint requests to Dr. William J. Hudspeth. Neuropsychometrics Laboratory, 415B Sanford Street, Radford, VA 24141.

0278-2626/93 $5.00

from simple sensations to complex cognitive processes (Regan, 1972; Hillyard, Picton, & Regan, 1978; Hillyard & Picton, 1979; John and Schwartz, 1978). The present work expands upon traditional methods that have been used to determine whether VEP indices reflect *interpretations* of complex visual stimuli (Beglieter & Porjesz, 1975; Beglieter, Porjesz, & Garozzo, 1979; Chapman, 1977; Chapman, McCrary, Chapman, & Bragdon, 1978; John, Herrington, & Sutton, 1967; John, 1977; Johnston and Chesney, 1974; Shelburne, 1973; Buchsbaum, Coppola, & Bittker, 1974; Tyler, Roemer, Harrison, & Thompson, 1973; Thatcher, 1977a,b; Roemer & Tyler, 1977). The general conclusions that arise from these particular studies show that VEP waveshapes are determined by the meaningful, rather than physical, attributes of visual stimuli. These studies also show that, with complex stimuli, observed changes in the VEP waveshape typically involve multiple peak components. Consequently, the entire waveshape (e.g., an envelope of 500+ msec duration) would appear to be essential in identifying specific perceptual or conceptual features in VEP waveshapes.

One of the significant aspects of human visual function is that the conceptual attributes of visual stimuli can be related to each other through intricate classification hierarchies, which are based upon experience with the similarities and dissimilarities among the forms (i.e., attributes) and functions encountered. The present experiments were designed to investigate the implication that VEP waveshapes reflect the meaningful relationships among stimulus objects and their attributes. This question, in turn, pointed to the need for formal principles by which the VEP waveshape can encode conceptual, perceptual, and sensory information. Modern studies in neurophysics (Nunez, 1981) suggest that the generation of EEG (i.e., VEPs) waves in cortical architectures have a characteristic property that provides a working hypothesis for the current studies: *The VEP waveshape is a linear product space, composed of N orthogonal waveshape components which are requisite in number to span an N-dimensional attribute space,* where attribute space is defined by the number and type of stimulus attributes (i.e., sensory, perceptual, or conceptual) that are contained within a stimulus set.

The foundations for the rationale, methods, and expected results in this study are based upon well-established principles and methods in mathematical psychology (Shepard, 1972; Degerman, 1972; Guttman, 1954; Rapaport & Fillenbaum, 1972; Künnapas, Mälhammar, & Svenson, 1964). Based upon these principles, it was first necessary to select a set of stimulus attributes that were sufficient in number to encompass the distinctions among sensory, perceptual, and conceptual operations. It was determined that an abstract conceptual attribute space could be defined by a stimulus set having a minimum of two dimensions, and no less than two exemplars in each dimension (see Discussion). Conservative

and meaningful stimulus attributes were chosen, i.e., those that had successfully been used in previous VEP and mathematical classification studies. As is shown below, the selected stimuli (e.g., green circle, green triangle, red circle, red triangle) met all of the criteria for an abstract (conceptual) classification set. The characteristics of form and color classifications have been described in previous work.

Continuous classification (scaling) procedures are used to define the relationships (similarities and differences) among perceptual stimuli within a single attribute domain. For example, when human subjects rated the similarities among different (n = 15) colors, the geometric configuration of their ratings described a color wheel, with complimentary colors (e.g., green & red) positioned on opposite sides of a unit circle (Guttman, 1954). It is tempting to imagine that this color wheel represents an absolute perceptual scale which is based upon basic neuronal mechanisms for color vision. However, it is significant that when human subjects rated the similarities among different (n = 24) color words, the geometric configuration of their ratings described a color wheel, with complimentary color words (e.g., "green" and "red") located on opposite sides of a unit circle (Rapaport & Fillenbaum, 1972). Thus, symbols (color words) and their referents (colors) were judged to have the same interstimulus relationships and, therefore, the same interpretation. Similarly, when human subjects rated the similarities among different (n = 7) geometric stimuli, the configuration of their ratings positioned circle, triangle, square and cross stimuli at the vertices of a tetrahedron structure in three-dimensional space (Künnapas et al., 1964).

Unlike continuous classification methods (e.g., perceptual relations), discrete classification methods are necessary for establishing relationships across two (or more) attribute domains, such as conjoined form and color attributes. While any two colors and any two forms could be used, it is obviously important to attain optimal separation between the endpoints for each attribute dimension. Therefore, the selected primary attributes in the current studies achieve this goal; e.g., green and red are perceptual opposites, and circle and triangle are primary nodes (apices) on a form tetrahedron. Therefore, if the current investigations do no more than replicate previous VEP results, a form–color classification by means of VEP waveshapes can be predicted with reasonable certainty because the four orthogonal stimuli used here entail strong linear dependencies that assure partial correlations (i.e., $r^2 \approx 50\%$) among VEP waveshapes that share common attributes.

METHODS

Stimulus classification model. Figure 1A presents the stimulus matrix used in the study. The stimuli that were presented to the subjects are shown in the cells of the stimulus matrix (e.g., C1F1, green circle; C2F1, red circle; C1F2, green triangle; C2F2, red triangle). Since

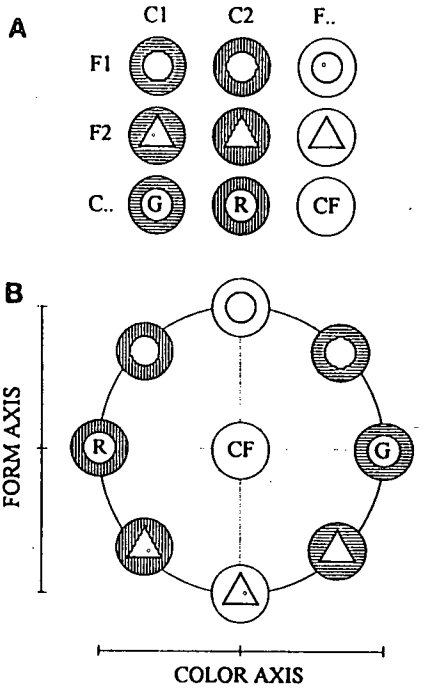

FIG. 1. (A) Orthogonal stimulus matrix used in the investigations. The cells of the stimulus matrix show the stimuli that were presented to the subjects (C1F1, green circle; C2F1, red circle; C1F2, green triangle, C2F2, red triangle). The primary color attributes are located in the column marginals C.. (C1, green; C2, red) and the primary form attributes are located in the row marginals F.. (F1, circle; F2, triangle). (B) A priori model by which the form and color features of the stimulus set were positioned on the circumference of a unit circle. The stimulus classification model, based on the stimulus matrix ($n = 8$), can be quantified with a list of sines and cosines, or transformed to degrees of arc, to define the stimulus classification vector (AS) which was used as the input (i.e., comparison) model for the statistical evaluation of transfer functions reported in the paper. Circle and triangle features are represented by geometric forms; green features have horizontal line backgrounds, whereas red features have vertical line backgrounds. Primary form features have white backgrounds, i.e., *no* color feature, whereas primary color features have appropriately indexed backgrounds and the letters G(reen) and R(ed) to indicate the *absence* of form features.

each stimulus is composed of two orthogonal attributes, estimates for the primary color attributes (C..) are located in the column marginals (C1, green; C2, red) of the stimulus matrix, and estimates for the primary form attributes (F..) are located in the row marginals (F1, circle; F2, triangle) of the stimulus matrix. Therefore, a full classification for the stimulus matrix can be determined from the proportional contribution of each attribute to the cells and marginals of the stimulus matrix. To make accurate hypothesis testing possible, the stimulus matrix was quantified to index the cell and marginal interrelationships (i.e., r^2 = proportional representation) on the circumference of a unit circle that provided a completely abstract interpretation (i.e., classification) of the stimulus set.

The unit circle model used in the present work can be constructed from a standard paradigm for discrete classifications: (a) when structure A (form) has $r = 2$ points (circle

and triangle) on $m = 1$ dimension, and (b) structure B (color) has $s = 2$ points (green and red) on $n = 1$ dimension, then (c) the Cartesian product, $A \times B$, will consist of $rs = 4$ points in $(n + m) = 2$ dimensions, thus producing a composite space with the two original structures located in orthogonal subspaces (adapted from Degerman, 1972, p. 198). Figure 1B presents the resulting unit circle model. The primary circle and triangle attributes represent *opposing* poles of the form (Y) dimension, and the primary green and red attributes represent *opposing* poles of the color (X) dimension. Insofar as the form and color dimensions are orthogonal, intermediate stimuli, i.e., those having conjoined form and color attributes, are linear composites (50%/50%) of the specific form–color attributes indexed. As can be seen in Fig. 1B, the stimulus matrix can optionally be defined by a list of sines and cosines (x, color; y, form) or by an equivalent list of degrees of arc, e.g., starting circle at 0° (top) and moving clockwise through green → triangle → red: (0.000, 1.000) = 0, (0.707, 0.707) = 45, (1.000, 0.000) = 90, (0.707, −0.707) = 135, (0.000, −1.000) = 180, (−0.707, −0.707) = 225, (−1.000, 0.000) = 270, and −0.707, 0.707) = 315 degrees, respectively. These values provided the quantitative definition for the attribute space (AS) (an eight-element vector). The methods described below show how the VEP data sets were transformed into a product space (PS) (an eight-element vector), which made direct comparisons with the AS vector possible.

Predictions. Despite the abstract representation inherent within the AS, the observed translations obtained from VEP waveshapes (e.g., in PS vectors), were free to vary between theoretical endpoints for concrete (sensory) and abstract (conceptual) operations. Thus, a completely concrete translation would reflect four nominally distinct stimuli that have no apparent similarities and would require four orthogonal VEP waveshape components. Conversely, a completely abstract translation recognizes all of the relationships within the AS, and would require only two orthogonal VEP waveshape components, as described by the a priori classification model presented in Fig. 1B. Intermediate solutions can be conceived (i.e., able to translate form but not color, or able to translate color but not form), and any such evidence will be noted.

Subjects. Eight (four male, four female), 19- to 35-year-old healthy college students were informed of the benefits and risks of participating in the study, and all signed an informed consent document before starting the experiment. All of the subjects had normal (including corrected) vision, as defined by their verbal reports. Further estimates of visual acuity were obtained during an information trial (described below) in which the subjects were familiarized with the sources and reduction of EEG artifacts (e.g., muscle and eye movement).

Stimulus set. The stimuli were computer-generated graphics with combined color and form features: green circle, red circle; green triangle, red triangle. Each stimulus was presented as a line drawing (i.e., not solid) on a high-resolution color monitor that had equated RGB luminance levels (using a Macbeth illuminometer). Thus, both form and color were defined by the same screen pixels that had the same luminance levels. The stimuli had equal areas, enclosed within a circumference of 33 mm, which subtended 1.26° of retinal arc at a viewing distance of 1.5 m (Graham, 1960).

Stimulus luminance levels were not measured because of adjustments made to control screen artifacts that occur on long-persistence CRT monitors. In total darkness, image onset and offset are characterized by propagating and decaying brightness levels, respectively. This artifact can distort stimulus brightness levels, as well as the duration of the stimulus on–off cycle. The artifact can be minimized or eliminated by increasing room illumination and decreasing CRT brightness. Through experimentation (three judges), we were able to fix satisfactory brightness levels that would (a) minimize the amount of room illumination needed to mask artifacts and (b) maximize the brightness of stimulus displays, short of triggering artifacts. There is the possibility that the sensitivity of experimental subjects differed slightly from that of the judges.

Apparatus and procedure. VEP recordings were obtained from eight locations of the

international 10/20 electrode system: C3, C4, T5, T6, P3, P4, O1, and O2 (Jasper, 1958). An Electro-Cap, International electrode cap was used to make scalp connections for referential (to linked earlobes) recordings with a 10-channel Beckman Accutrace EEG instrument. One extra channel was used to record eye movement artifacts with bipolar transorbital electrodes, placed diagonally, from midline (1.5 cm above naison) to the left edge of the zygomatic arch. The EEG amplifiers had a nominal bandpass of 0.5–40.0 Hz. Computer software provided for stimulus presentations of 5-msec duration at a rate of 0.5 Hz. VEP recordings were digitized at 400 Hz, until 200 conversions (e.g., 500 msec) were completed for all channels. Eye artifact records were automatically compared with a preset artifact threshold value (described below) and, accordingly, the VEPs were either saved on disk or rejected and replaced with acceptable VEPs for the same stimulus.

The subjects were comfortably seated in a semidarkened room and allowed 20 min for dark adaptation. During this period, the subjects observed their ongoing EEG activities on a CRT screen, so that they could see the effects of various sources of artifact (e.g., muscle tension, body and eye movements). During the relaxation phase of this instruction, a 1-min EEG recording was obtained to calculate the mean and variance of voltage measurements from the eye-artifact electrode, which were used to set the initial artifact threshold within the range, $Z = \pm 2.0\sigma - \pm 2.5\sigma$. Finally, the subjects were asked to judge the clarity (i.e., acuity) of the computer images, and any last-minute changes (i.e., installing or removing glasses or contact lenses) were completed at that time.

At the start of the experiment, subjects were asked to attend to a single illuminated pixel on the computer monitor, where each stimulus was presented in small blocks (five trials each). Each stimulus block was repeated in counterbalanced order to distribute fatigue and habituation equally across the stimuli. Data acquisition continued until 50 artifact-free VEPs were saved for each stimulus.

Preanalysis. The final VEP data were prepared for analysis in the following ways: (a) single-trial records were visually inspected to exclude records with residual eye or muscle artifacts; (b) all VEPs were truncated to 100 points (5 msec/point) with an adjacent-point averaging routine to preserve the 500-msec epoch length; and (c) each averaged VEP was smoothed with a three-point running average and then transformed to a z-score scale (Mean $= 0$, $\sigma = 1.0$) to equate the amplitude (root mean square) energy of VEPs for all subjects and electrodes (John et al., 1972; John, 1977; Hudspeth & Jones, 1977; Thatcher, 1977a,b). The distribution and range of obtained z-score values are described in Figs. 2 and 3 (captions).

Each subject's raw data provided four averaged VEPs for each of eight recording electrodes. A VEP data set, the primary analysis matrix, was constructed for each electrode and subject. Each VEP data set contained eight averaged VEPs to reflect each stimulus in the AS vector. These included four averaged VEPs for the stimuli presented to the subjects (i.e., Cells of Fig. 1A) and four averaged VEPs derived from averaging pairs of VEPs that shared a primary attribute (Marginals of Fig. 1A: circle, triangle; green, red). A CATEGORIZED group VEP data set was calculated for each electrode by averaging VEP data sets across subjects.

The unit circle model assumes that the origin of the VEP data set is equal to zero (Figs. 1A and 1B: CF, the grand mean of the stimulus matrix) which, in the case of VEP data sets, is a condition that does not obtain without correction. For example, the eight VEP waveshapes, within each data set, shared a common waveshape, which was calculated as the average VEP waveshape for each electrode (EVEP). The EVEP is an exogenous waveshape component that reflects the luminance fluctuations of visual stimulation. In addition, the EVEP reflects the unique status of each anatomical region (i.e., electrode), as well as the current state of the subject. By definition, the EVEP does not contain information about stimulus attributes, and it can safely be defined as an index for the *operational* state of different brain regions. Since the present studies were interested in the *content* states within

different brain regions, the EVEP waveshape in each data set was removed to construct deviation VEP (ΔVEP) data sets that had a common origin equal to zero. These calculations were accomplished by subtracting the EVEP for each electrode from each of the eight VEPs for the same electrode. In all, 72 ΔVEP data sets (eight electrodes for eight subjects + 1 group mean) were prepared for analysis. All statistical analyses reported in this paper were carried out in SYSTAT V. 5.0, using the MGLH, CORR, FACTOR, and STATS modules (Wilkenson, 1990). Greenhouse–Geiser and Huynh–Feldt corrections were obtained for all repeated measurements ANOVAs, and the adjusted probabilities are reported as, p_{HF}.

Analysis of VEP waveshapes. The following analyses were used to determine the extent to which the unit circle model predicted the gross morphology of the averaged ΔVEP waveshapes. The ΔVEPs for the primary form and color features (i.e., circle vs. triangle and green vs. red) were assumed to provide estimates for the primary features used here. The primary hypothesis provides the assumptions and the expected configuration for the eight ΔVEP waveshapes. If the underlying neural generation system implemented an abstract conceptual solution, the ΔVEP waveshapes would necessarily conform to the underlying neurodynamics. The unit circle model directly requests a solution that entails *orthogonality* and *opposing* attributes on *two dimensions*. Therefore, the ΔVEP waveshapes would have to reflect this solution within a set of waveshape dynamics that are compatible with that solution. Realistically, there is only one VEP waveshape index that is fully compatible with this solution. In this instance, the underlying generator systems would have to use a phase-encoded mechanism. Therefore, the expected results can be described as (a) the ΔVEP waveshapes for the poles of the form dimension (i.e., circle vs. triangle) are expected to be highly similar and inversely related; (b) ΔVEP waveshapes for the poles of the color dimension (i.e., green vs. red) are also expected to be similar and inversely related; and (c) since the form and color dimensions are on orthogonal axes, it is prudent to expect little, or no, similarity between form and color ΔVEP waveshapes.

Preliminary inspection of the data showed that ΔVEP waveshape correlations and signal strength indices varied across stimuli and electrode locations. The following statistical analyses were carried out to evaluate these variations. Pearson product–moment correlations were computed between ΔVEP waveshape pairs for the form (e.g., circle × triangle), color (e.g., green × red), and the orthogonal (e.g., form × color) axes in each data set. All correlations were squared (r^2) and then normalized with a log transformation. These analyses produced an 8 × 3 (electrodes × axes) matrix of normalized r^2 values for each subject. A repeated-measures ANOVA was used to determine whether there were systematic differences in ΔVEP waveshape predictabilities (normalized): (a) between electrodes, (b) within axis comparisons (e.g., form, color, and orthogonal); or (c) that depended upon specific electrodes and axes.

Analysis of VEP signal strength. The signal strength index was computed as the power contained in each 100-point ΔVEP: (a) The 100 points in each ΔVEP were squared (x^2); (b) summed over 100 points (Σx^2); and (c) the final index was calculated as: sqrt(Σx^2). The signal strength indices for the circle and triangle VEPs were averaged as an index for the form dimension, and the green and red indices were averaged as an index for the color dimension. These analyses produced an 8 × 2 (electrodes × dimensions) matrix of signal strength indices for each subject. A repeated-measurements ANOVA was used to determine whether there were systematic differences in ΔVEP signal strength (a) between electrodes; (b) within the form and color dimensions; or (c) that depended upon specific electrodes and dimensions.

Analysis of transfer functions. The following analyses were used to determine the extent to which the 72 observed ΔVEP data sets reproduced the AS vector (Fig. 1B). These analyses were used to evaluate the magnitude and error variance of the transfer function described above. To make direct comparisons possible, the 72 ΔVEP data sets were converted to observed PS vectors.

Each ΔVEP data set was placed in computer memory with eight ΔVEPs in columns and

100 digitized time points in rows. A correlation matrix was then computed between the eight column combinations. The resulting correlation matrix was submitted to principal components analysis and then rotated to the varimax criterion (discussion of methods: Guertin & Bailey, 1970; John, 1977; John, Walker, Cawood, Rush, & Gehrman, 1972; Hudspeth & Jones, 1977; Hudspeth, 1985, 1990; Hudspeth, 1993; Thatcher, 1977a,b). The programs were designed to retain component loadings for the two largest eigenvalues. Of the 72 varimax component analyses computed, 2 components were sufficient to account for no less than 90.0% of the variance in 61 of the data sets and no less than 83.6% of the variance in the remaining 11 data sets. These results could be duplicated with principal components, equamax or quartimax rotations, and with multidimensional scaling methods. The varimax component which accounted for most of the variance in the form (X) dimension was used as an estimate for the cosines, and the second component, the color (Y) dimension, was used as an estimate for the sines of a unit circle, respectively.

The 72 observed PS output vectors (i.e., subjects and group means) were calculated by converting the varimax component loadings (i.e., sine and cosine estimates) to degrees of arc. The angular offset of the eight ΔVEPs was removed so that the origin of the circle ΔVEP was set to 0°, and the remaining ΔVEPs were free to vary around the unit circle. These analyses produced an 8 × 8 (electrodes × angles) matrix for each subject.

The magnitude of the transfer function between AS and PS was estimated from the correlations between the AS vector and the 72 observed PS output vectors. Both Pearson product-moment and Guttmann MU2 coefficients were computed for each of these estimates. All of the MU2 coefficients were equal to 1.0, and the average of all Pearson coefficients was 0.99. The correlation findings were sufficiently clear that further analyses seemed unnecessary. Nevertheless, the 72 observed PS vectors contained small and systematic deviations from expected locations in the AS vector. These deviations were obtained by vector subtraction ($(PS_i - AS_i)$, where $i = 2$–8; column 1 not used). These analyses produced an 8 × 7 (electrodes × angles) matrix for each subject. A repeated-measurements ANOVA was used to determine whether there were systematic differences in transfer function errors (a) between electrodes; (b) within 7 octants of the unit circle (i.e., the AS vector); or (c) that depended upon specific electrodes and octant positions.

RESULTS

Evaluation of VEP waveshapes. Figure 2 presents CATEGORIZED EVEP and ΔVEP waveshapes for the GROUP data sets. The EVEP waveshape for each electrode is shown (thick tracing) in columns 1 and 2 of Fig. 2 to emphasize the fact that the EVEP was the only origin for calculating ΔVEP waveshapes for each electrode. Column 1 shows that the circle and triangle VEP waveshapes exhibit clear symmetrical deviations around the EVEPs for each electrode. Similarly, column 3 shows that the red and green VEP waveshapes also exhibit symmetrical deviations around the EVEPs for each electrode. Columns 3, 4, and 5 show ΔVEP waveshape pairs for each electrode and attribute dimension, e.g., form (circle vs. triangle), color (green vs. red), and orthogonal (form vs. color) axes. The quantitative index for the relationship between ΔVEP waveshape pairs was r^2, the percentage of shared variance, which is printed next to each of the ΔVEP waveshape pairs. Since the direction (sign) of the waveshape pair relationship was specified in the classification model, the sign of the original correlations has been appended to the r^2

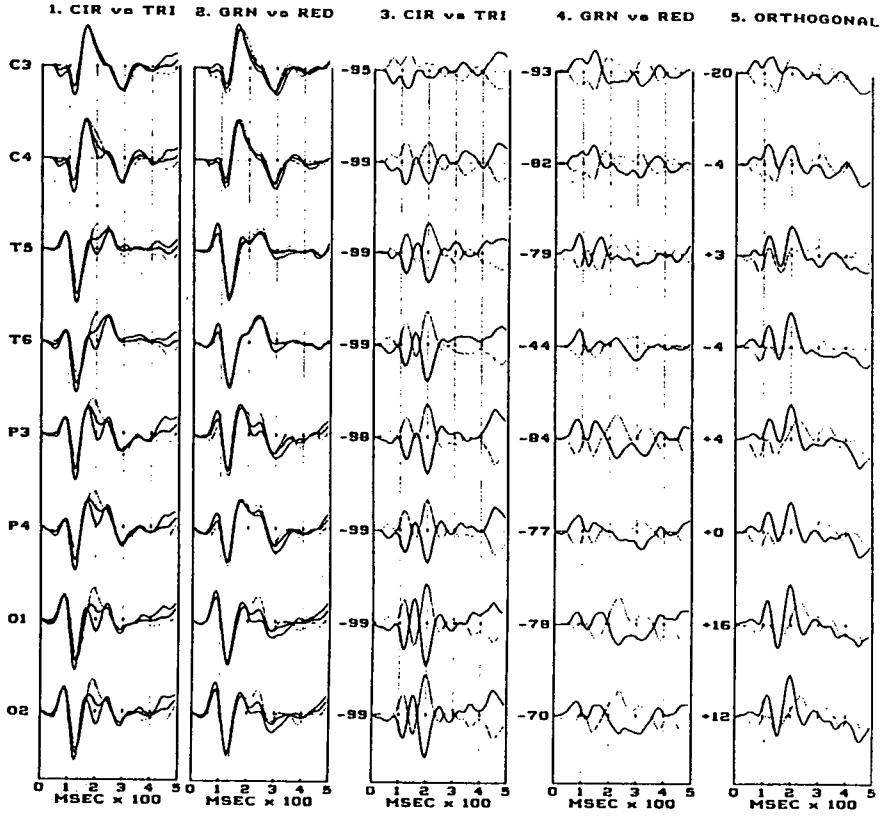

FIG. 2. Depicts CATEGORIZED VEP waveshape pairs for the form (Fig. 2, column 1: circle vs. triangle) and color (Fig. 2, column 2: red vs. green) axes. Note that in columns 1 and 2 the form and color VEP waveshapes deviate symmetrically around the EVEP average (shown as a thick line) for each electrode. When the EVEP averages were removed at each electrode site, ΔVEP waveshape pairs for the form (Fig. 2, column 3) axis and the color (Fig. 2, column 4) axis were nearly identical and 180° out of phase. In contrast, ΔVEP waveshape pairs for the orthogonal axes (Fig. 2, column 5: form vs. color) were effectively uncorrelated. The sign and magnitude of the squared correlation coefficients (r^2) for each pair of ΔVEP waveshapes is presented to the left of the tracings for each recording location and axis comparison (form, color, and orthogonal). Each VEP and ΔVEP waveshape was based on averages from eight subjects, and contained $N \approx 740$ waveforms (i.e., stimulus presentations). Each waveshape pair is composed of dotted and solid line tracings that identify primary attributes named in each figure heading (columns 3–5). In all cases, the first named attribute is the dotted line, and the second named attribute is the solid line. The epoch length of each waveshape was 500 msec, using 100 points with 5 msec/point resolution. The amplitude of all VEP waveshapes was equated by transformation to a z-score scale with a Mean = 0, and $\sigma = 1.0$. The maximum peak-to-peak amplitude of VEP waveshapes varied, over the scalp, from $Z = \pm 2.61$ to $Z = \pm 2.98$. The maximum peak-to-peak amplitude of ΔVEP waveshapes varied, over the scalp, from $Z = \pm 1.16$ to $Z = \pm 1.53$. Please note that the Scaling factor for ΔVEP waveshapes is 50% larger than that for VEP waveshapes.

values. Please note that for the orthogonal axis, form waveshapes were computed as the average of the circle and (sign inverted) triangle ΔVEPs, and color waveshapes were computed as the average of the green and (sign inverted) red ΔVEPs.

As can be seen, the unit circle model (e.g., AS) predicted ΔVEP waveshape pairs with considerable accuracy. Figure 2, column 3, shows that ΔVEP waveshape pairs for the form axis (circle vs. triangle) were nearly identical (r^2 = 95–99%) and 180° out of phase. Similarly, Fig. 2, column 4, shows that the ΔVEP waveshapes for the color axis (green vs. red) were also similar (r^2 = 44–93%) and 180° out of phase. Finally, Fig. 2, column 5, shows that the ΔVEP waveshape pairs on orthogonal axes were effectively unrelated (r^2 = 0–20%). An inspection of all subject ΔVEPs revealed the same findings, and Table 1 provides a summary of the r^2 values for each subject, electrode, primary axis; i.e., form, color, and orthogonal. The data presented in Table 1 show that all of the subjects exhibited the same ΔVEP waveshape pair relationships as the GROUP averages presented in Fig. 2, columns 3–5.

Since the CATEGORIZED ΔVEP waveshape pairs provided such strong evidence that the waveshapes contained stable classification components for form and color information, a complementary hypothesis was advanced to determine whether the robust ΔVEP classification symmetries could be broken by randomizing subject VEP waveshapes produced by visual stimulation and then recompute the marginal averages, EVEP and ΔVEP waveshapes, as before. It followed, therefore, that if RANDOMIZED VEP waveshapes produce ΔVEPs that have little, or no, classification information, it would seem safe to conclude that the original CATEGORIZED waveshapes contained stable classification information. The complementary hypothesis was tested by: (1) randomly assigning each subject's VEPs for green circle, green triangle, red circle, and red triangle to the cells (C1F1, C1F2, C2F1, C2F2) of the stimulus matrix. The randomization was constrained so that, with four stimuli for each of eight subjects, the new cell VEP averages contained two waveshapes for each stimulus in the set; (2) recalculating the primary marginal (i.e., F1, circle; F2, triangle; C1, green; C2, red) VEP waveshapes; (3) recalculating the EVEP averages (CF); and then (4) recalculating the ΔVEP waveshape pairs.

The RANDOMIZED EVEP (same as EVEP for CATEGORIZED data), VEP and ΔVEP waveshapes shown in Fig. 3 provided decidedly different results than those obtained with CATEGORIZED waveshapes. It can be seen that the input of randomized VEP waveshapes clearly degraded the strong polar symmetries (180° phase-reversal) observed with CATEGORIZED waveshapes. Whereas a few brain regions exhibit moderate r^2 values, on the average, r^2 values for RANDOMIZED ΔVEP waveshape pairs were 75.9% lower than CATEGORIZED ΔVEPs on the

TABLE 1
Squared-Correlations for ΔVEP Waveshape Pairs (r^2 = %)

Ss	C3	C4	T5	T6	P3	P4	O1	O2	Sm
				(A) Form axis (circle vs. triangle)					
S1	−82	−99	−99	−99	−96	−99	−97	−98	−96
S2	−85	−88	−99	−99	−99	−99	−99	−94	−95
S3	−94	−99	−99	−99	−99	−99	−99	−99	−98
S4	−92	−96	−99	−99	−97	−98	−98	−99	−97
S5	−99	−99	−97	−99	−99	−99	−98	−99	−98
S6	−83	−98	−99	−99	−94	−97	−99	−99	−96
S7	−97	−98	−93	−99	−97	−98	−98	−99	−97
S8	−99	−99	−99	−99	−99	−99	−99	−99	−99
Em	−91	−97	−98	−99	−97	−98	−98	−98	−97
				(B) Color axis (green vs. red)					
S1	−99	−99	−99	−75	−87	−99	−63	−58	−84
S2	−89	−88	−99	−87	−99	−99	−99	−97	−94
S3	−95	−99	−99	−99	−99	−99	−77	−57	−90
S4	−97	−93	−81	−74	−87	−85	−58	−49	−78
S5	−99	−99	−93	−99	−99	−99	−85	−99	−96
S6	−99	−87	−99	−99	−97	−93	−99	−99	−96
S7	−88	−66	−92	−71	−91	−88	−91	−99	−86
S8	−87	−99	−99	−99	−99	−99	−99	−85	−96
Em	−94	−91	−95	−88	−94	−95	−84	−80	−90
				(C) Orthogonal axes (form vs. color)					
S1	−1	0	−7	−22	−4	−4	−12	−19	8
S2	0	−4	−2	2	0	1	8	13	4
S3	−19	−3	−6	−9	0	0	1	0	4
S4	−10	−2	0	−2	−2	−1	0	0	2
S5	0	0	18	0	2	0	5	4	4
S6	2	0	−3	0	6	2	3	7	2
S7	−36	0	0	−10	−5	−1	3	0	6
S8	−33	−2	2	−1	−4	0	14	0	7
Em	12	1	4	6	4	1	6	5	5

Note. Ss(S1–S8), subjects; Em, electrode means; Sm, subject means.

form axis (circle vs. triangle), and 48.0% lower than CATEGORIZED ΔVEPs on the color axis (green vs. red). There were no differences between r^2 values for RANDOMIZED and CATEGORIZED ΔVEP waveshape pairs on ORTHOGONAL axes. These findings clearly show that RANDOMIZED ΔVEP waveshape pairs do not contain classification information. Therefore, the CATEGORIZED findings appear to be robust because they do contain stable form and color waveshape components.

An analysis of the CATEGORIZED data showed that (a) there was no overall difference in ΔVEP waveshape pair r^2 values obtained from different electrodes ($F(7, 56) = 0.95$, $p = 0.48$); (b) there were substantial

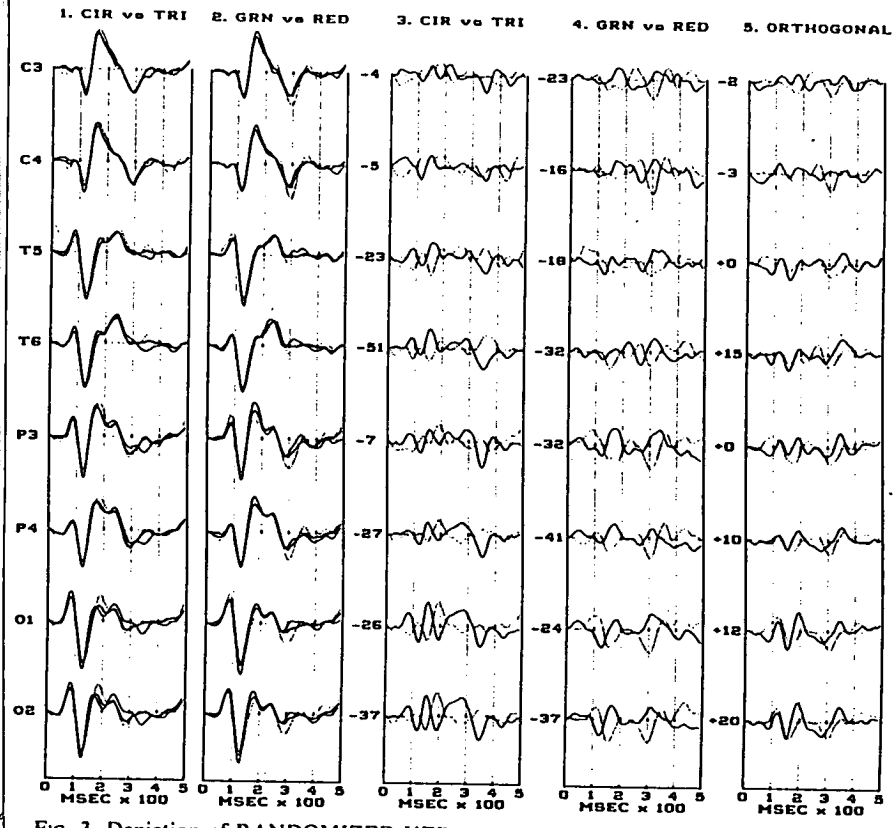

FIG. 3. Depiction of RANDOMIZED VEP waveshapes and ΔVEP waveshape pairs for the GROUP mean (MN). Column 1 depicts the averaged EVEP waveshape for each electrode (thick line) along with the form (circle vs. triangle) VEP waveshapes, that do not deviate symmetrically around their respective EVEP averages. Column 2 presents the EVEP waveshapes for each electrode (thick line) along with the color (green vs. red) VEP waveshapes, that also do not deviate symmetrically around the EVEP average. Column 3 depicts the ΔVEP waveshape pairs for the form (circle vs. triangle) axis that do not have the same waveshapes. Column 4 shows the ΔVEP waveshape pairs for the color (green vs. red) axis that also do not have the same waveshapes. Column 5 presents ΔVEP waveshape pairs for the orthogonal axes (form vs. color). The sign and magnitude of the squared correlation coefficients (r^2) is shown next to each ΔVEP waveshape pair. The parameters, data tracings, and scaling factors are the same as those reported in Fig. 2.

differences among r^2 values for ΔVEP waveshape pairs on the form, color, and orthogonal axes ($F(1, 56) = 2380.96$, $p_{HF} = 0.0009$). A single degree-of-freedom polynomial contrast showed that there were no differences between r^2 values for waveshape pairs on the form and color axes and that these values were significantly higher than the r^2 values on the orthogonal axes ($F(8, 56) = 656.40$, $p = 0.0009$); (c) the r^2 values for ΔVEP waveshape pairs on the form, color, and orthogonal axes depended

TABLE 2
ΔVEP Waveshape Signal Strength Index (Z)

Ss	C3	C4	T5	T6	P3	P4	O1	O2	Sm
				(A) Form VEPs					
S1	18.0	21.2	55.0	59.4	43.8	42.7	55.5	57.2	44.0
S2	44.5	38.4	33.5	30.2	33.4	22.8	23.6	25.5	31.4
S3	26.7	25.5	38.2	43.0	47.4	49.0	47.2	49.4	40.8
S4	23.2	27.0	53.1	45.8	45.3	42.9	56.8	53.4	43.4
S5	29.4	32.1	30.0	30.7	34.3	28.9	39.3	36.5	32.6
S6	17.4	28.8	20.6	35.3	21.9	27.2	25.9	29.7	25.8
S7	39.1	43.4	32.8	39.2	37.1	34.7	29.0	34.0	36.1
S8	40.2	46.5	29.0	29.5	29.8	23.7	15.2	23.6	29.6
Em	29.8	32.9	36.5	39.1	36.6	35.2	36.6	38.7	35.7
				(B) Color VEPs					
S1	29.2	27.2	42.1	44.3	38.5	34.6	40.9	40.4	37.1
S2	46.0	38.3	24.7	20.9	34.0	25.8	28.5	29.1	30.9
S3	27.7	26.0	26.5	20.8	30.3	26.0	32.2	27.5	27.1
S4	27.2	25.1	42.3	31.6	37.7	33.8	41.8	35.0	34.3
S5	23.7	22.7	25.9	26.9	27.3	26.3	30.5	25.3	26.0
S6	27.2	20.7	23.7	19.6	24.1	23.6	25.5	28.3	24.0
S7	32.5	29.1	33.0	23.3	33.1	28.2	23.3	25.4	28.4
S8	30.2	24.2	34.0	23.7	33.6	26.6	15.8	26.7	26.8
Em	30.5	26.7	31.7	26.4	32.3	28.1	29.8	29.7	29.4

Note. Ss(S1–S8), subjects; Em, electrode means; Sm, subject means.

upon specific electrode locations ($F(14, 112) = 2.38$, $p_{HF} = 0.006$). This finding was primarily due to the fact that the left central electrode (C3) provided significantly lower r^2 values for the form axis and slightly higher r^2 values for the orthogonal axes. The reliability of these findings for individual subjects can be verified by the results presented in Table 1.

Evaluation of VEP signal strength. Table 2 presents signal strength indices for the form (A) and color (B) ΔVEP waveshapes obtained from each subject (S1–S8) and electrode derivation (C3–O2). As can be seen in Table 2, the signal strength of form ΔVEPs was generally larger than color ΔVEPs. An analysis of these data showed that (a) there were no differences in ΔVEP signal strength among different electrodes ($F(7, 56) = 0.39$, $p = 0.90$), (b) the signal strength of form ΔVEP waveshapes was significantly larger than that of color ΔVEP waveshapes ($F(1, 56) = 41.68$; $p = 0.0009$), and (c) there was marginal evidence that form and color ΔVEP signal strength indices depended upon specific electrode locations ($F(7, 56) = 1.93$; $p = 0.08$). However, these could not be verified with multiple comparisons tests.

Evaluation of transfer function. Figure 4A presents the observed GROUP PS vectors for each electrode derivation. As can be seen, these

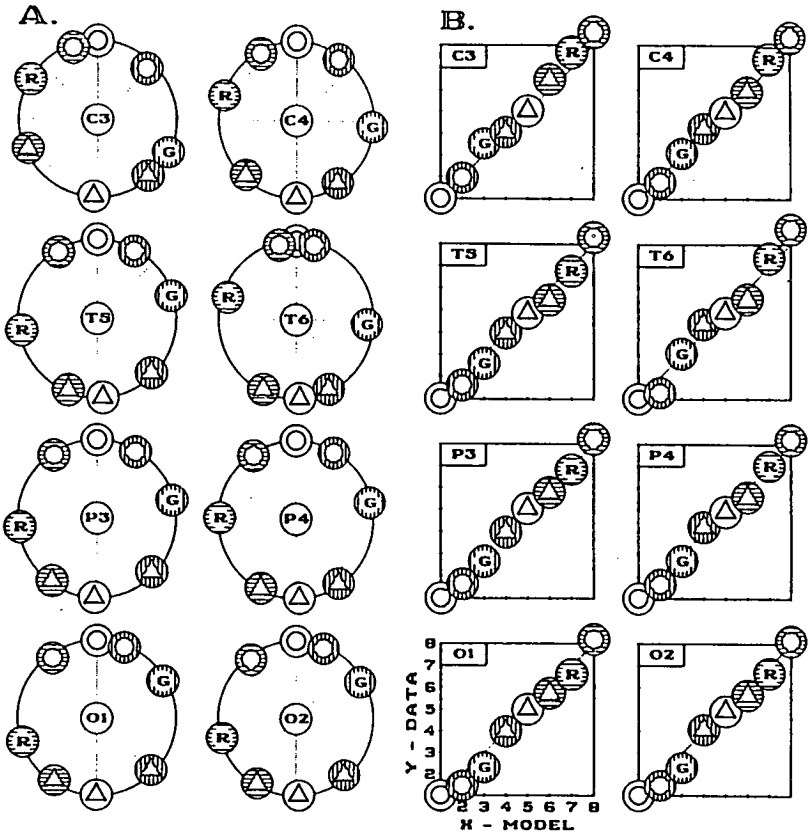

FIG. 4. Graphic analysis of the transfer function, AS = PS, for each electrode location. Observed output PS vectors for each electrode location. These results show how well the observed ΔVEP data sets reproduce the unit circle classification. (B) Scattergrams based upon the expected, AS, vector (MODEL = x axis) and the averaged observed, PS, vectors (DATA = y axis). The statistical analyses for these data are presented in text, and the specific values can be found in Tables 3A and 3B. Circle, triangle, green, and red features are represented by the same graphic coding scheme as that described for Fig. 1.

findings closely approximate the unit circle model specified in the AS vector. Figure 4B provides a scatterplot for each electrode, in which the AS and PS vectors are graphed on the X (MODEL) and Y (DATA) axes, respectively. Nonparametric and parametric correlations between the AS and the 72 observed PS vectors ranged from 0.98 to 1.0, to yield an average predictability of 99%. Table 3A shows that the quality (r^2) of observed transfer functions was reliable across subjects and electrodes.

Table 3B presents the average deviations (i.e., angular error) from the expected position of the eight ΔVEPs on the octants of the unit circle. As can be seen, the average error for all electrodes and subjects was only 1°. However, there were systematic errors which require discussion. An

TABLE 3
Anatomical Distribution of Transfer Functions

(A) Squared correlations between PS and AS vectors (r^2 = %)

Ss	C3	C4	T5	T6	P3	P4	O1	O2	Sm
S1	98	99	99	99	99	99	98	98	98
S2	99	99	99	99	99	99	99	99	99
S3	99	99	99	98	99	99	99	98	99
S4	99	99	99	99	99	99	99	99	99
S5	99	99	99	99	99	99	99	99	99
S6	98	99	99	99	99	99	99	99	99
S7	98	99	99	98	99	99	99	99	99
S8	98	98	99	99	99	99	99	99	99
Em	98	99	99	99	99	99	99	99	99

(B) Distribution of PS errors (PS°–AS°)

AS°	C3	C4	T5	T6	P3	P4	O1	O2	Am
0	0	0	0	0	0	0	0	0	0
45	−10	−14	−8	−18	−13	−12	−18	−18	−14
90	9	2	1	8	4	0	−8	−4	2
135	1	1	−2	12	−1	2	−1	4	2
180	−1	−1	−0	−0	0	−1	2	1	0
225	11	4	−1	−4	7	0	2	−0	2
270	12	3	2	10	4	3	−5	−1	4
315	16	16	10	17	10	11	10	9	12
Em	5	2	0	4	2	1	−2	−1	1

Note. Ss(S1–S8), subjects; Em, electrode mean; Sm, subject mean; Am, Angular mean.

analysis of these data showed the following: (a) There were no differences in the distribution of errors among electrodes ($F(7, 56) = 1.00, p = 0.44$). (b) The average distribution of errors differed significantly within the stimulus set ($F(6, 336) = 46.95; p_{HF} = 0.0009$). Single degree-of-freedom contrasts showed that these differences were primarily due to the fact that the ΔVEPs for the circle stimuli (i.e., green and red circles) were less influenced by color variations and, consequently, were mislocated 13° closer to the circle, positioned at 0° (green: $F(1, 56) = 141.35, p = 0.0009$; red: $F(1, 56) = 68.49, p = 0.0009$). (c) The angular error in positioning each of the eight ΔVEPs did not depend upon specific electrode locations ($F(42, 336) = 1.32, p_{HF} = 0.15$).

DISCUSSION

We can now return to the original questions posed in this paper. Recordings of VEP waveshapes were obtained from human observers during visual stimulation with an abstract stimulus set, an AS. The PS indices extracted from the ΔVEP waveshapes reflected an abstract interpretation

of the AS with very high accuracy. These results provide substantial evidence that the abstract content of human visual processing can, within certain limitations, be identified in VEP waveshape recordings. Insofar as the transfer functions, PS = AS, were consistent with an abstract classification, absolute sensory and perceptual attributes were clearly not evident. Therefore, the specificity of ΔVEP waveshapes for the attributes of the stimuli were *relative* to the present set of stimuli.

Although the results for individual subjects were robust, this does not mean that every subject had the same VEP waveshapes. To the contrary, these and other studies show that, with complex stimuli, the VEP waveshape exhibits the properties of other biological markers for subject identity (e.g., voice print, fingerprint, eye print, DNA): (a) everyone has VEP waveshapes; (b) there appear to be nominally distinct families of the VEP waveshape pattern with, perhaps, predictable incidence rates in the population; and (c) in the end, the actual VEP waveshape is unique for the individual. Therefore, Tables 1–3 provide the essential evidence that the results (i.e., waveshape pair correlations, signal strength indices, and transfer functions) were not only reliable across subjects, these data also show that the results were somewhat more robust for within-subject calculations.

The primary hypothesis predicted that the obtained VEP waveshapes would be a linear composite of N orthogonal waveshape components that were required to account for the N-dimensional AS (orthogonal stimulus matrix) presented to the subjects. The a priori model (i.e., Fig. 1B) provided an abstract (conceptual) interpretation of the AS vector that required only two bipolar dimensions. Transfer functions that were returned in ΔVEP PS vectors provided several challenging conclusions. (a) Eighty-six to ninety percent of the variance in ΔVEP data sets ($n = 8$ waveshapes) could be attributed to two bipolar dimensions (i.e., varimax components), having the same configuration as the AS model. These findings provided excellent support for the primary hypothesis. (b) Ten to fourteen percent of the variance in ΔVEP data sets was due to unknown sources of error. (c) The exogenous EVEP waveshape component, which was removed from VEP data sets, constituted an additional VEP waveshape component and suggests that the primary hypothesis should be modified to reflect this source of variability. Therefore, the primary hypothesis can be restated: *The VEP waveshape is a linear product space, composed of $N + 1$ orthogonal waveshape components (and error variance) which are requisite in number to span an N-dimensional attribute space and a single observer dimension (i.e., experimental intrusion).*

The most fascinating finding in these studies was the fact that the AS model predicted major ΔVEP waveshape phase relationships. While varimax components analysis was only used to quantify these relationships

in PS vectors, there can be little doubt that the averaged ΔVEP waveshapes (Fig. 2) directly exhibited all of the properties predicted by the AS model. Where the model defined stimulus features as opposing poles of an attribute dimension (i.e., form *or* color), ΔVEP waveshapes were nearly identical and 180° out of phase. Similarly, where the model defined form *and* color attributes on orthogonal axes (i.e., x, y), ΔVEP waveshapes for the form and color axes were effectively uncorrelated (average $r^2 = 5\%$).

These results provided strong evidence that the original VEP waveshapes contained valid form and color classification information. To validate these findings further, a complimentary hypothesis posed that if the original VEP waveshapes contained valid form and color classification information, then the entire classification could be broken by reconstructing the ΔVEP waveshapes from a RANDOMIZED set of VEP waveshapes that included exemplars for every stimulus in the set. This analysis revealed sets of *random* ΔVEP waveshapes that had little or no form and color classification information. Therefore, the primary hypothesis, and the derived AS model, appear to accurately reflect the allocation of VEP waveshape resources (PS) when human observers view stimuli that constitute an abstract classification.[1]

The present results raise a number of provocative questions concerning the organization of neuronal generator systems that can exhibit the VEP waveshape dynamics observed in this work. Specifically, the averaged EVEP and ΔVEP waveshapes shown in Fig. 2 lead directly to the infer-

[1] The impression has been voiced that the findings obtained in this study may be due to linear calculation dependencies that inevitably lead to artifactual robustness. This impression arises from attempts to decompose the complexity of the entire VEP classification into simpler operations, for example, calculating ΔVEP waveshapes for one axis at a time. From this perspective, constraining the analysis to two VEP waveshapes, the mean of *any pair* of VEP waveshapes is centered within the range of the waveshape pair, and the ΔVEP waveshapes will deviate symmetrically around *their* mean. Then, if successive axes (pairs of VEP waveshapes) are examined in turn, each ΔVEP waveshape pair will deviate symmetrically around *their* mean. Finally, this view concludes that, if the above were true, then a completely *random* set of VEP waveshape patterns would *always* yield perfect ΔVEP classifications. This simplified interpretation misrepresents the procedures used in the present studies. The present procedures were based upon eight VEP waveshapes, and to achieve the ΔVEP classifications reported here, the EVEPs were centered *between all eight VEP waveshapes simultaneously*. As soon as four or more VEP waveshapes are entered into the analysis, artifactual classifications cannot be found. ΔVEP classifications only emerge if they exist in the original input VEP waveshapes. For example, calculate the mean (i.e., EVEP) for any four values, using a two-dimensional approach with two axes and two values/axis. The computed deviation scores are *always* symmetrical around EVEP when the *four input* values are symmetrical (i.e., classified input: $x = (5, 15)$, $y = (5, 15)$; mean = 10; and output: $x = (-5, +5)$, $y = (-5, +5)$), but the computed deviation scores are *never* symmetrical around the mean when the *four input* values are asymmetrical (i.e., unclassified input: $x = (5, 15)$, $y = (10, 15)$; Mean = 11.25; and output: $x = (-6.25, +3.75)$, $y = (-1.25, +3.75)$).

ence that the underlying neuronal system(s) *use* phase-encoded eigenfunctions to represent the abstract classification. The significance of this coding (representational) scheme becomes evident when the possible neural origins of EVEP and ΔVEP waveshape components are considered. Nunez (1981) provides a detailed account of the neurophysical bases for different wave phenomena in the central nervous system, and the calculations that are required to define such wave phenomena are extensive, nontrivial, and obviously not carried out in the current studies. However, the observed behavior of the EVEP and ΔVEP waveshapes suggest the hypothesis that these waveshape components could reflect *propagated* and *standing* waves, respectively, that arise from distinct anatomical compartments (Nunez, 1981, pp. 315–346).

For example, the observed EVEP waveshapes are analogous to propagated waves that occur when information is transmitted through the pathways and associated nuclei of the retino–striate system. The successive peaks of the VEP waveshape are typically associated with activation of each of the neuronal links associated with the retino–striate system and, thus, the analogy makes partial sense.

Similarly, the observed behavior of ΔVEP waveshapes are analogous to cortical standing waves, in which propagated waves are mapped into the visual cortex where the cortical architecture is organized as a sheet of dipole columns that are interlaced with interneurons and horizontal fibers. The consequence of this horizontal organization enables cortical architectures to support standing waves that entail the algebraic sum of N orthogonal waveshapes (i.e., eigenfunctions) which are sufficient in number to match N input stimuli (adapted from Nunez, 1981). While this part of the analogy also seems to be consistent with the observed behavior of ΔVEP waveshapes, the author would point to two additional properties that are not currently part of the standing wave model. First, the standing wave model employs eigenfunctions for the algebraic summation of *successive* input stimuli. The current studies show that the cortex also supports *simultaneous* eigenfunctions that reflect conjoined stimulus attributes. Second, the standing wave model does not currently support the influence of experience and learning, by which a myriad of distinct stimuli (or attributes) attain abstract equivalences that simplify (reduce dimensionality) the organization, plasticity, and recall of cognitive representations. These revisions entail the operational definitions for AS and PS, as exemplified in the primary hypothesis used here.

During the period this paper was in the review process, Young and Yamane (1992) have shown that the discharge pattern of neuronal populations in monkey inferotemporal cortex encode human faces (n = 27 photographs) in two dimensions that served to identify specific individuals (i.e., laboratory personnel), based upon the configuration of facial attributes. They used analytic methods similar to those presented in the cur-

rent paper, and they concluded that facial classifications were based upon a sparse (i.e., distributed) population code. Since the discharge pattern of neuronal populations is determined by the algebraic sum of dendritic slow potentials, it seems likely that their findings may also entail phase-encoded eigenfunctions that reveal phase reversals for the polar endpoints of two facial attribute dimensions. Obviously, the accuracy of this inference requires empirical validation.

The results obtained in the current studies, and in the findings of Young and Yamane (1992), are based upon the method of conjoint similarities and differences. As Young and Yamane observe, this method provides stronger hypothesis-testing strategies than traditional methods. In the current studies, for example, it can be seen that the use of orthogonalized stimulus attributes (i.e., AS) and structural analysis clearly obviate alternative interpretations (e.g., differences in attention or arousal) that have previously been offered to exclude perceptual or cognitive interpretations of VEP data. It seems likely that this method can provide robust predictions and tests of hypotheses concerning cerebral processes that underlie a number of specific psychological processes. Thus, in the present work, the method tends to increase the certainty that cerebral mechanisms are engaged in *cognitive work*, rather than support functions.

As a concluding question: What do the present findings reveal about the brain mechanisms of cognitive function, especially with regard to conceptual classifications? The results have addressed two fundamental issues. First, the results imply that the underlying neural generator system has, at minimum, the functional capacities of a cortical sheet, and it seems likely that these correspond to traditional cortical systems. Second, the results also implied that the underlying neural generator system used phase-encoded eigenfunctions to represent an abstract classification. These two observations lead to the conclusion that the relevant cortical systems can be understood from the perspectives of *computational anatomy* (Hudspeth, 1985, 1990; Hudspeth, 1993; Hudspeth & Pribram, 1990, 1992; John & Schwartz, 1978; Pribram, 1991; Schwartz, 1980, 1990). Assuming that such a model operated in the present instance, the author would have to conclude that product spaces are represented by computational systems and that the observed ΔVEP waveshape changes merely provided the inferences concerning the nature of cortical computation.

REFERENCES

Beglieter, H., & Porjesz, B. 1975. Evoked brain potentials as indicators of decision making. *Science*, **187**, 754–755.

Begleiter, H., Porjesz, B., & Garozzo, R. 1979. Visual evoked potentials and affective ratings of semantic stimuli. In: H. Begleiter (Ed.), *Evoked brain potentials and behavior*. New York: Plenum.

Buchsbaum, M., Coppola, R., & Bittker, T. E. 1974. Differential effects of congruence, stimulus meaning and information on early and late components of the averaged evoked response. *Neuropsychologia*, **12**, 533–545.

Chapman, R. M. 1977. Methods of evoked potentials analysis in linguistic research. In: D. A. Otto (Ed.), *Multidisciplinary perspectives in event-related potential research*. Washington, DC: Government Printing Office.

Chapman, R. M., McCrary, J. W., Chapman, J. A., & Bragdon, H. R. 1978. Brain responses related to semantic meaning. *Brain and Language*, **5**, 195–205.

Degerman, R. L. 1972. The geometric representation of some simple structures. In: R. N. Shepard, A. K. Romney, and S. B. Nerlove (Eds.), *Multidimensional scaling: Theory and applications in the behavioral sciences*. New York: Seminar Press.

Graham, C. H. 1960. Visual perception. In: S. S. Stevens (ed.), *Handbook of experimental psychology*. New York: Wiley.

Guttman, L. 1954. A new approach to factor analysis: The radex. In: P. F. Lazarsfield (Ed.), *Mathematical thinking in the social sciences*. Glencoe, IL: Free Press.

Guertin, W. H., & Bailey, J. P., Jr. 1970. *Introduction to modern factor analysis*. Ann Arbor: Edwards Brothers.

Hillyard, S. A., Picton, T. W., & Regan, D. 1978. Sensation, perception and attention: Analysis using ERPs. In: *Event-related brain potentials in man*. E. Callaway, P. Tueting, & S. H. Koslow (Eds.), New York: Academic Press.

Hillyard, S. A., & Picton, W. T. 1979. Event-related brain potentials and selective information processing in man. In: J. E. Desmedt (Ed.), *Progress in clinical neurophysiology, cognitive components in cerebral event-related potentials and selective attention*. Basel: Karger. Vol. 6.

Hudspeth, W. J., & Jones, G. B. 1977. Neural models for short-term memory: A quantitative study of averaged evoked potential waveform. *Neuropsychologia*, **16**, 201–212.

Hudspeth, W. J. 1985. Developmental neuropsychology: Functional implications of quantitative EEG maturation. *Journal of Clinical and Experimental Neuropsychology*, **7**, 606. [Abstract]

Hudspeth, W. J. 1990. VEPs and dimensions of visual perception. *Proceedings of the Fifth International Congress of Psychophysiology*, 132. [Abstract]

Hudspeth, W. J. 1993. Knowledge representation in brain electrical activity. In: D. S. Levine and M. Aparicio (Eds.), *Neural Networks for Knowledge Representation and Inference*. Hillsdale, NJ: Lawrence Erlbaum Associates. In press.

Hudspeth, W. J., & Pribram, K. H. 1990. Stages of brain and cognitive maturation. *Journal of Educational Psychology*, **82**, 880–883.

Hudspeth, W. J., & Pribram, K. H. 1992. Psychophysiological indices of cerebral maturation. *International Journal of Psychophysiology*, **12**, 19–29.

Jasper, H. H. 1958. The ten–twenty electrode system of the International Federation. *Electroencephalography and Clinical Neurophysiology*, **10**, 371–375.

John, E. R., Herrington, R. N., & Sutton, S. 1967. Effects of visual form on the evoked response. *Science*, **155**, 1439–1442.

John, E. R., Walker, P., Cawood, D., Rush, M., & Gehrmann, J. 1972. Mathematical identification of brain states applied to classification of drugs. *International Review of Neurobiology*, **15**, 273–347.

John, E. R. 1977. *Functional neuroscience: Neurometrics: Clinical applications of quantitative neurophysiology*. Hillsdale, NJ: Erlbaum. Vol. 2.

John, E. R., & Schwartz, E. L. 1978. The neurophysiology of information processing and cognition. *Annual Review of Psychology*, **29**, 1–29.

Johnston, V. L., & Chesney, G. L. 1974. Electrophysiological correlates of meaning. *Science*, **186**, 944–946.

Künnapas, T. Mälhammar, G., & Svenson, O. 1964. Multidimensional ratio scaling and

multidimensional similarity of simple geometric figures. *Scandanavian Journal of Psychology*, 5, 249–256.

Nunez, P. L. 1981. *Electrical fields of the brain: Neurophysics of EEG*. New York: Oxford Univ. Press.

Rapoport, A., & Fillenbaum, S. 1972. An experimental study of semantic structure. In: A. K. Romney, R. N. Shepard, & S. B. Nerlove (Eds.), *Multidimensional scaling: Theory and applications in the behavioral sciences*. New York: Seminar Press. Vol. 2.

Pribram, K. H. 1991. *Brain and perception: Holonomy and structure in figural processing*. Hillsdale, NJ. Erlbaum.

Regan, D. 1972. *Evoked potentials in psychology, sensory physiology and clinical medicine*. New York: Wiley–Interscience.

Roemer, R. A., & Teyler, T. J. 1977. Auditory evoked potential asymmetries related to word meaning. In: J. Desmedt (Ed.), *Progress in clinical neurophysiology: Language and hemispheric specialization in man: Cerebral event-related potentials*. Basel: Karger. Vol. 3.

Schwartz, E. L. 1980. Computational anatomy and functional architecture of striate cortex: A spatial mapping approach to perceptual coding. *Vision Research*, 20, 645–669.

Schwartz, E. L. 1990. *Computational neuroscience*. Cambridge: MIT–Bradford Press.

Shelburne, S. A., Jr. 1973. Visual evoked response to language stimuli in children with reading disabilities. *Electroencephalography and Clinical Neurophysiology*, 34, 135–143.

Shepard, R. N. 1972. The taxonomy of some principal types of data and multidimensional methods for their analysis. In: R. N. Shepard, A. K. Romney, & S. B. Nerlove (Eds.), *Multidimensional scaling: Theory and applications in the behavioral sciences*. New York: Seminar Press.

Thatcher, R. W. 1977a. Evoked potential correlates of delayed letter matching. *Behavioral Biology*, 19, 1–23.

Thatcher, R. W. 1977b. Evoked potential correlates of hemispheric lateralization during semantic information processing. In: S. Harnand, R. W. Doty, L. Goldstein, J. Jaynes, & G. Krauthamer (Eds.), *Lateralization of the nervous system*. New York: Academic Press.

Tyler, T. J., Roemer, R. A., Harrison, T. F., & Thompson, R. F. 1973. Human scalp recorded evoked-potential correlates of linguistic stimuli. *Bulletin of the Psychonomic Society*, 1, 333–334.

Wilkenson, L. 1990. *Systat: The system for statistics (Ver. 5.0)*. Evanston, IL: Systat, Inc.

Young, M. P., & Yamane, S. 1992. Sparse population coding of faces in the inferotemporal cortex. *Science*, 256, 1327–1331.

BRAIN AND COGNITION 21, 226–246 (1993)

Neuroelectric Concepts: Form–Color Classification

WILLIAM J. HUDSPETH

Neuropsychometrics Laboratory and Department of Psychology, Radford University

Visual event-related potentials (VEPs) were recorded from the scalp of human observers who viewed an orthogonal stimulus set, consisting of four stimuli, each of which had two attributes: a form (circle or triangle) and a color (green or red). The stimulus set was represented by an a priori stimulus classification model, defined by positions (i.e., degrees of arc) on a unit circle that specified the relationships among the form and color features. An analysis of VEP deviation waveshapes (ΔVEP: deviations around average VEP for each electrode) showed that the a priori unit circle model predicted morphologies of the ΔVEP waveshapes, as well as the overall relationships between waveshapes obtained for the form and the color attributes. Further analyses demonstrated that individual ΔVEP waveshapes for color and for form were located on the circumference of a unit circle at the positions (angle) specified by the a priori model. The studies show that formal modeling of the way humans classify stimulus attributes provides a quantitative and predictive model of the way VEPs become classified and organized according to psychological principles.

INTRODUCTION

Visual pattern recognition can be analyzed according to hierarchical (i.e., top–down) neural processes that organize concepts, percepts, and sensory images. The question to be addressed in this report is: When records of brain electrical activities are obtained during visual stimulation, do the obtained measurements reflect sensory imaging, perceptual constancies, or the conceptual classification of the stimuli presented to experimental subjects?

Scalp recordings of visual event-related potentials (VEPs) have been used to investigate a number of functions of the human visual system, from simple sensations to complex cognitive processes (Regan, 1972; Hillyard, Picton, & Regan, 1978; Hillyard & Picton, 1979; John and Schwartz, 1978). The present work expands upon traditional methods that have been used to determine whether VEP indices reflect *interpretations* of complex visual stimuli (Beglieter & Porjesz, 1975; Beglieter, Porjesz, & Garozzo, 1979; Chapman, 1977; Chapman, McCrary, Chapman, & Bragdon, 1978; John, Herrington, & Sutton, 1967; John, 1977; Johnston and Chesney, 1974; Shelburne, 1973; Buchsbaum, Coppola, & Bittker, 1974; Tyler, Roemer, Harrison, & Thompson, 1973; Thatcher, 1977a,b; Roemer & Tyler, 1977). The general conclusions that arise from these particular studies show that VEP waveshapes are determined by the meaningful, rather than physical, attributes of visual stimuli. These studies also show that, with complex stimuli, observed changes in the VEP waveshape typically involve multiple peak components. Consequently, the entire waveshape (e.g., an envelope of 500+ msec duration) would appear to be essential in identifying specific perceptual or conceptual features in VEP waveshapes.

One of the significant aspects of human visual function is that the conceptual attributes of visual stimuli can be related to each other through intricate classification hierarchies, which are based upon experience with the similarities and dissimilarities among the forms (i.e., attributes) and functions encountered. The present experiments were designed to investigate the implication that VEP waveshapes reflect the meaningful relationships among stimulus objects and their attributes. This question, in turn, pointed to the need for formal principles by which the VEP waveshape can encode conceptual, perceptual, and sensory information. Modern studies in neurophysics (Nunez, 1981) suggest that the generation of EEG (i.e., VEPs) waves in cortical architectures have a characteristic property that provides a working hypothesis for the current studies: *The VEP waveshape is a linear product space, composed of N orthogonal waveshape components which are requisite in number to span an N-dimensional attribute space*, where attribute space is defined by the number and type of stimulus attributes (i.e., sensory, perceptual, or conceptual) that are contained within a stimulus set.

The foundations for the rationale, methods, and expected results in this study are based upon well-established principles and methods in mathematical psychology (Shepard, 1972; Degerman, 1972; Guttman, 1954; Rapaport & Fillenbaum, 1972; Künnapas, Mälhammar, & Svenson, 1964). Based upon these principles, it was first necessary to select a set of stimulus attributes that were sufficient in number to encompass the distinctions among sensory, perceptual, and conceptual operations. It was determined that an abstract conceptual attribute space could be defined by a stimulus set having a minimum of two dimensions, and no less than two exemplars in each dimension (see Discussion). Conservative

I thank Robert Thatcher for many challenging discussions while developing the quantitative model reported in this work. I am grateful to Karl Pribram and Lauren Gerbrandt for their interest, comments, and criticisms while preparing the manuscript. I also thank Ms. Amy Garrett for helping me develop the geometric algorithms and Ms. Candy Disch for preparing subjects in the experiments. Address reprint requests to Dr. William J. Hudspeth, Neuropsychometrics Laboratory, 415B Sanford Street, Radford, VA 24141.

0278-2626/93 $5.00

and meaningful stimulus attributes were chosen, i.e., those that had successfully been used in previous VEP and mathematical classification studies. As is shown below, the selected stimuli (e.g., green circle, green triangle, red circle, red triangle) met all of the criteria for an abstract (conceptual) classification set. The characteristics of form and color classifications have been described in previous work.

Continuous classification (scaling) procedures are used to define the relationships (similarities and differences) among perceptual stimuli within a single attribute domain. For example, when human subjects rated the similarities among different (n = 15) colors, the geometric configuration of their ratings described a color wheel, with complimentary colors (e.g., green & red) positioned on opposite sides of a unit circle (Guttman, 1954). It is tempting to imagine that this color wheel represents an absolute perceptual scale which is based upon basic neuronal mechanisms for color vision. However, it is significant that when human subjects rated the similarities among different (n = 24) color words, the geometric configuration of their ratings described a color wheel, with complimentary color words (e.g., "green" and "red") located on opposite sides of a unit circle (Rapaport & Fillenbaum, 1972). Thus, symbols (color words) and their referents (colors) were judged to have the same interstimulus relationships and, therefore, the same interpretation. Similarly, when human subjects rated the similarities among different (n = 7) geometric stimuli, the configuration of their ratings positioned circle, triangle, square and cross stimuli at the vertices of a tetrahedron structure in three-dimensional space (Künnapas et al., 1964).

Unlike continuous classification methods (e.g., perceptual relations), discrete classification methods are necessary for establishing relationships across two (or more) attribute domains, such as conjoined form and color attributes. While any two colors and any two forms could be used, it is obviously important to attain optimal separation between the endpoints for each attribute dimension. Therefore, the selected primary attributes in the current studies achieve this goal; e.g., green and red are perceptual opposites, and circle and triangle are primary nodes (apices) on a form tetrahedron. Therefore, if the current investigations do no more than replicate previous VEP results, a form–color classification by means of VEP waveshapes can be predicted with reasonable certainty because the four orthogonal stimuli used here entail strong linear dependencies that assure partial correlations (i.e., $r^2 \approx 50\%$) among VEP waveshapes that share common attributes.

METHODS

Stimulus classification model. Figure 1A presents the stimulus matrix used in the study. The stimuli that were presented to the subjects are shown in the cells of the stimulus matrix (e.g., C1F1, green circle; C2F1, red circle; C1F2, green triangle; C2F2, red triangle). Since each stimulus is composed of two orthogonal attributes, estimates for the primary color attributes (C..) are located in the column marginals (C1, green; C2, red) of the stimulus matrix, and estimates for the primary form attributes (F..) are located in the row marginals (F1, circle; F2, triangle) of the stimulus matrix. Therefore, a full classification for the stimulus matrix can be determined from the proportional contribution of each attribute to the cells and marginals of the stimulus matrix. To make accurate hypothesis testing possible, the stimulus matrix was quantified to index the cell and marginal interrelationships (i.e., r^2 = proportional representation) on the circumference of a unit circle that provided a completely abstract interpretation (i.e., classification) of the stimulus set.

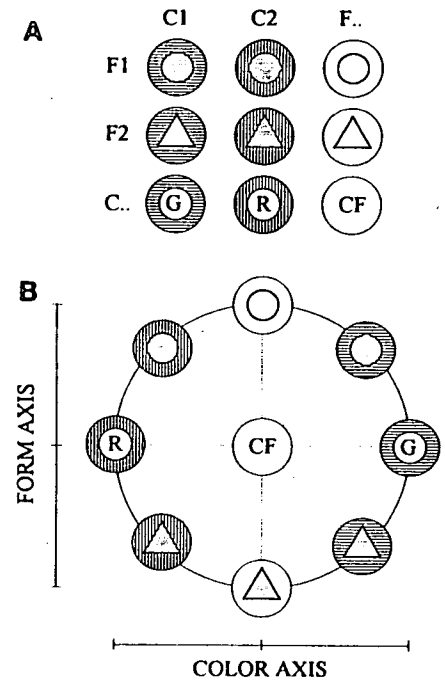

FIG. 1. (A) Orthogonal stimulus matrix used in the investigations. The cells of the stimulus matrix show the stimuli that were presented to the subjects (C1F1, green circle; C2F1, red circle; C1F2, green triangle, C2F2, red triangle). The primary color attributes are located in the column marginals C.. (C1, green; C2, red) and the primary form attributes are located in the row marginals F.. (F1, circle; F2, triangle). (B) A priori model by which the form and color features of the stimulus set were positioned on the circumference of a unit circle. The stimulus classification model, based on the stimulus matrix (n = 8), can be quantified with a list of sines and cosines, or transformed to degrees of arc, to define the stimulus classification vector (AS) which was used as the input (i.e., comparison) model for the statistical evaluation of transfer functions reported in the paper. Circle and triangle features are represented by geometric forms; green features have horizontal line backgrounds, whereas red features have vertical line backgrounds. Primary form features have white backgrounds, i.e., *no* color feature, whereas primary color features have appropriately indexed backgrounds and the letters G(reen) and R(ed) to indicate the *absence* of form features.

The unit circle model used in the present work can be constructed from a standard paradigm for discrete classifications: (a) when structure A (form) has r = 2 points (circle

and triangle) on $m = 1$ dimension, and (b) structure B (color) has $s = 2$ points (green and red) on $n = 1$ dimension, then (c) the Cartesian product, $A \times B$, will consist of $rs = 4$ points in $(n + m) = 2$ dimensions, thus producing a composite space with the two original structures located in orthogonal subspaces (adapted from Degerman, 1972, p. 198). Figure 1B presents the resulting unit circle model. The primary circle and triangle attributes represent *opposing* poles of the form (Y) dimension, and the primary green and red attributes represent *opposing* poles of the color (X) dimension. Insofar as the form and color dimensions are orthogonal, intermediate stimuli, i.e., those having conjoined form and color attributes, are linear composites (50%/50%) of the specific form–color attributes indexed. As can be seen in Fig. 1B, the stimulus matrix can optionally be defined by a list of sines and cosines (x, color; y, form) or by an equivalent list of degrees of arc, e.g., starting circle at 0° (top) and moving clockwise through green → triangle → red: (0.000, 1.000) = 0, (0.707, 0.707) = 45, (1.000, 0.000) = 90, (0.707, −0.707) = 135, (0.000, −1.000) = 180, (−0.707, −0.707) = 225, (−1.000, 0.000) = 270, and −0.707, 0.707) = 315 degrees, respectively. These values provided the quantitative definition for the attribute space (AS) (an eight-element vector). The methods described below show how the VEP data sets were transformed into a product space (PS) (an eight-element vector), which made direct comparisons with the AS vector possible.

Predictions. Despite the abstract representation inherent within the AS, the observed translations obtained from VEP waveshapes (e.g., in PS vectors), were free to vary between theoretical endpoints for concrete (sensory) and abstract (conceptual) operations. Thus, a completely concrete translation would reflect four nominally distinct stimuli that have no apparent similarities and would require four orthogonal VEP waveshape components. Conversely, a completely abstract translation recognizes all of the relationships within the AS, and would require only two orthogonal VEP waveshape components, as described by the a priori classification model presented in Fig. 1B. Intermediate solutions can be conceived (i.e., able to translate form but not color, or able to translate color but not form), and any such evidence will be noted.

Subjects. Eight (four male, four female), 19- to 35-year-old healthy college students were informed of the benefits and risks of participating in the study, and all signed an informed consent document before starting the experiment. All of the subjects had normal (including corrected) vision, as defined by their verbal reports. Further estimates of visual acuity were obtained during an information trial (described below) in which the subjects were familiarized with the sources and reduction of EEG artifacts (e.g., muscle and eye movement).

Stimulus set. The stimuli were computer-generated graphics with combined color and form features: green circle, red circle; green triangle, red triangle. Each stimulus was presented as a line drawing (i.e., not solid) on a high-resolution color monitor that had equated RGB luminance levels (using a Macbeth illuminometer). Thus, both form and color were defined by the same screen pixels that had the same luminance levels. The stimuli had equal areas, enclosed within a circumference of 33 mm, which subtended 1.26° of retinal arc at a viewing distance of 1.5 m (Graham, 1960).

Stimulus luminance levels were not measured because of adjustments made to control screen artifacts that occur on long-persistence CRT monitors. In total darkness, image onset and offset are characterized by propagating and decaying brightness levels, respectively. This artifact can distort stimulus brightness levels, as well as the duration of the stimulus on–off cycle. The artifact can be minimized or eliminated by increasing room illumination and decreasing CRT brightness. Through experimentation (three judges), we were able to fix satisfactory brightness levels that would (a) minimize the amount of room illumination needed to mask artifacts and (b) maximize the brightness of stimulus displays, short of triggering artifacts. There is the possibility that the sensitivity of experimental subjects differed slightly from that of the judges.

Apparatus and procedure. VEP recordings were obtained from eight locations of the international 10/20 electrode system: C3, C4, T5, T6, P3, P4, O1, and O2 (Jasper, 1958). An Electro-Cap, International electrode cap was used to make scalp connections for referential (to linked earlobes) recordings with a 10-channel Beckman Accutrace EEG instrument. One extra channel was used to record eye movement artifacts with bipolar transorbital electrodes, placed diagonally, from midline (1.5 cm above naison) to the left edge of the zygomatic arch. The EEG amplifiers had a nominal bandpass of 0.5–40.0 Hz. Computer software provided for stimulus presentations of 5-msec duration at a rate of 0.5 Hz. VEP recordings were digitized at 400 Hz, until 200 conversions (e.g., 500 msec) were completed for all channels. Eye artifact records were automatically compared with a preset artifact threshold value (described below) and, accordingly, the VEPs were either saved on disk or rejected and replaced with acceptable VEPs for the same stimulus.

The subjects were comfortably seated in a semidarkened room and allowed 20 min for dark adaptation. During this period, the subjects observed their ongoing EEG activities on a CRT screen, so that they could see the effects of various sources of artifact (e.g., muscle tension, body and eye movements). During the relaxation phase of this instruction, a 1-min EEG recording was obtained to calculate the mean and variance of voltage measurements from the eye-artifact electrode, which were used to set the initial artifact threshold within the range, $Z = \pm 2.0\sigma - \pm 2.5\sigma$. Finally, the subjects were asked to judge the clarity (i.e., acuity) of the computer images, and any last-minute changes (i.e., installing or removing glasses or contact lenses) were completed at that time.

At the start of the experiment, subjects were asked to attend to a single illuminated pixel on the computer monitor, where each stimulus was presented in small blocks (five trials each). Each stimulus block was repeated in counterbalanced order to distribute fatigue and habituation equally across the stimuli. Data acquisition continued until 50 artifact-free VEPs were saved for each stimulus.

Preanalysis. The final VEP data were prepared for analysis in the following ways: (a) single-trial records were visually inspected to exclude records with residual eye or muscle artifacts; (b) all VEPs were truncated to 100 points (5 msec/point) with an adjacent-point averaging routine to preserve the 500-msec epoch length; and (c) each averaged VEP was smoothed with a three-point running average and then transformed to a z-score scale (Mean = 0, $\sigma = 1.0$) to equate the amplitude (root mean square) energy of VEPs for all subjects and electrodes (John et al., 1972; John, 1977; Hudspeth & Jones, 1977; Thatcher, 1977a,b). The distribution and range of obtained z-score values are described in Figs. 2 and 3 (captions).

Each subject's raw data provided four averaged VEPs for each of eight recording electrodes. A VEP data set, the primary analysis matrix, was constructed for each electrode and subject. Each VEP data set contained eight averaged VEPs to reflect each stimulus in the AS vector. These included four averaged VEPs for the stimuli presented to the subjects (i.e., Cells of Fig. 1A) and four averaged VEPs derived from averaging pairs of VEPs that shared a primary attribute (Marginals of Fig. 1A: circle, triangle; green, red). A CATEGORIZED group VEP data set was calculated for each electrode by averaging VEP data sets across subjects.

The unit circle model assumes that the origin of the VEP data set is equal to zero (Figs. 1A and 1B: CF, the grand mean of the stimulus matrix) which, in the case of VEP data sets, is a condition that does not obtain without correction. For example, the eight VEP waveshapes, within each data set, shared a common waveshape, which was calculated as the average VEP waveshape for each electrode (EVEP). The EVEP is an exogenous waveshape component that reflects the luminance fluctuations of visual stimulation. In addition, the EVEP reflects the unique status of each anatomical region (i.e., electrode), as well as the current state of the subject. By definition, the EVEP does not contain information about stimulus attributes, and it can safely be defined as an index for the *operational* state of different brain regions. Since the present studies were interested in the *content* states within

different brain regions, the EVEP waveshape in each data set was removed to construct deviation VEP (ΔVEP) data sets that had a common origin equal to zero. These calculations were accomplished by subtracting the EVEP for each electrode from each of the eight VEPs for the same electrode. In all, 72 ΔVEP data sets (eight electrodes for eight subjects + 1 group mean) were prepared for analysis. All statistical analyses reported in this paper were carried out in SYSTAT V. 5.0, using the MGLH, CORR, FACTOR, and STATS modules (Wilkenson, 1990). Greenhouse–Geiser and Huynh–Feldt corrections were obtained for all repeated measurements ANOVAs, and the adjusted probabilities are reported as, p_{HF}.

Analysis of VEP waveshapes. The following analyses were used to determine the extent to which the unit circle model predicted the gross morphology of the averaged ΔVEP waveshapes. The ΔVEPs for the primary form and color features (i.e., circle vs. triangle and green vs. red) were assumed to provide estimates for the primary features used here. The primary hypothesis provides the assumptions and the expected configuration for the eight ΔVEP waveshapes. If the underlying neural generation system implemented an abstract conceptual solution, the ΔVEP waveshapes would necessarily conform to the underlying neurodynamics. The unit circle model directly requests a solution that entails *orthogonality* and *opposing* attributes on *two dimensions*. Therefore, the ΔVEP waveshapes would have to reflect this solution within a set of waveshape dynamics that are compatible with that solution. Realistically, there is only one VEP waveshape index that is fully compatible with this solution. In this instance, the underlying generator systems would have to use a phase-encoded mechanism. Therefore, the expected results can be described as (a) the ΔVEP waveshapes for the poles of the form dimension (i.e., circle vs. triangle) are expected to be highly similar and inversely related; (b) ΔVEP waveshapes for the poles of the color dimension (i.e., green vs. red) are also expected to be similar and inversely related; and (c) since the form and color dimensions are on orthogonal axes, it is prudent to expect little, or no, similarity between form and color ΔVEP waveshapes.

Preliminary inspection of the data showed that ΔVEP waveshape correlations and signal strength indices varied across stimuli and electrode locations. The following statistical analyses were carried out to evaluate these variations. Pearson product–moment correlations were computed between ΔVEP waveshape pairs for the form (e.g., circle × triangle), color (e.g., green × red), and the orthogonal (e.g., form × color) axes in each data set. All correlations were squared (r^2) and then normalized with a log transformation. These analyses produced an 8 × 3 (electrodes × axes) matrix of normalized r^2 values for each subject. A repeated-measures ANOVA was used to determine whether there were systematic differences in ΔVEP waveshape predictabilities (normalized): (a) between electrodes, (b) within axis comparisons (e.g., form, color, and orthogonal); or (c) that depended upon specific electrodes and axes.

Analysis of VEP signal strength. The signal strength index was computed as the power contained in each 100-point ΔVEP: (a) The 100 points in each ΔVEP were squared (x^2); (b) summed over 100 points (Σx^2); and (c) the final index was calculated as: sqrt(Σx^2). The signal strength indices for the circle and triangle VEPs were averaged as an index for the form dimension, and the green and red indices were averaged as an index for the color dimension. These analyses produced an 8 × 2 (electrodes × dimensions) matrix of signal strength indices for each subject. A repeated-measurements ANOVA was used to determine whether there were systematic differences in ΔVEP signal strength (a) between electrodes; (b) within the form and color dimensions; or (c) that depended upon specific electrodes and dimensions.

Analysis of transfer functions. The following analyses were used to determine the extent to which the 72 observed ΔVEP data sets reproduced the AS vector (Fig. 1B). These analyses were used to evaluate the magnitude and error variance of the transfer function described above. To make direct comparisons possible, the 72 ΔVEP data sets were converted to observed PS vectors.

Each ΔVEP data set was placed in computer memory with eight ΔVEPs in columns and 100 digitized time points in rows. A correlation matrix was then computed between the eight column combinations. The resulting correlation matrix was submitted to principal components analysis and then rotated to the varimax criterion (discussion of methods: Guertin & Bailey, 1970; John, 1977; John, Walker, Cawood, Rush, & Gehrman, 1972; Hudspeth & Jones, 1977; Hudspeth, 1985, 1990; Hudspeth, 1993; Thatcher, 1977a,b). The programs were designed to retain component loadings for the two largest eigenvalues. Of the 72 varimax component analyses computed, 2 components were sufficient to account for no less than 90.0% of the variance in 61 of the data sets and no less than 83.6% of the variance in the remaining 11 data sets. These results could be duplicated with principal components, equamax or quartimax rotations, and with multidimensional scaling methods. The varimax component which accounted for most of the variance in the form (X) dimension was used as an estimate for the cosines, and the second component, the color (Y) dimension, was used as an estimate for the sines of a unit circle, respectively.

The 72 observed PS output vectors (i.e., subjects and group means) were calculated by converting the varimax component loadings (i.e., sine and cosine estimates) to degrees of arc. The angular offset of the eight ΔVEPs was removed so that the origin of the circle ΔVEP was set to 0°, and the remaining ΔVEPs were free to vary around the unit circle. These analyses produced an 8 × 8 (electrodes × angles) matrix for each subject.

The magnitude of the transfer function between AS and PS was estimated from the correlations between the AS vector and the 72 observed PS output vectors. Both Pearson product-moment and Guttmann MU2 coefficients were computed for each of these estimates. All of the MU2 coefficients were equal to 1.0, and the average of all Pearson coefficients was 0.99. The correlation findings were sufficiently clear that further analyses seemed unnecessary. Nevertheless, the 72 observed PS vectors contained small and systematic deviations from expected locations in the AS vector. These deviations were obtained by vector subtraction ($(PS_i - AS_i)$, where i = 2–8; column 1 not used). These analyses produced an 8 × 7 (electrodes × angles) matrix for each subject. A repeated-measurements ANOVA was used to determine whether there were systematic differences in transfer function errors (a) between electrodes; (b) within 7 octants of the unit circle (i.e., the AS vector); or (c) that depended upon specific electrodes and octant positions.

RESULTS

Evaluation of VEP waveshapes. Figure 2 presents CATEGORIZED EVEP and ΔVEP waveshapes for the GROUP data sets. The EVEP waveshape for each electrode is shown (thick tracing) in columns 1 and 2 of Fig. 2 to emphasize the fact that the EVEP was the only origin for calculating ΔVEP waveshapes for each electrode. Column 1 shows that the circle and triangle VEP waveshapes exhibit clear symmetrical deviations around the EVEPs for each electrode. Similarly, column 3 shows that the red and green VEP waveshapes also exhibit symmetrical deviations around the EVEPs for each electrode. Columns 3, 4, and 5 show ΔVEP waveshape pairs for each electrode and attribute dimension, e.g., form (circle vs. triangle), color (green vs. red), and orthogonal (form vs. color) axes. The quantitative index for the relationship between ΔVEP waveshape pairs was r^2, the percentage of shared variance, which is printed next to each of the ΔVEP waveshape pairs. Since the direction (sign) of the waveshape pair relationship was specified in the classification model, the sign of the original correlations has been appended to the r^2

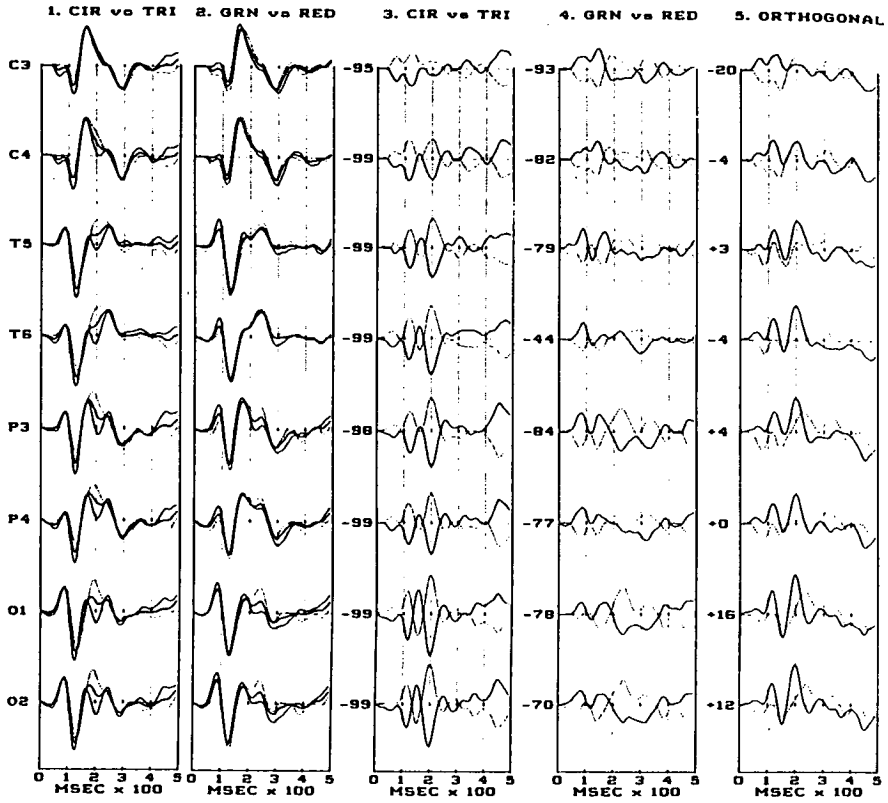

FIG. 2. Depicts CATEGORIZED VEP waveshape pairs for the form (Fig. 2, column 1: circle vs. triangle) and color (Fig. 2, column 2: red vs. green) axes. Note that in columns 1 and 2 the form and color VEP waveshapes deviate symmetrically around the EVEP average (shown as a thick line) for each electrode. When the EVEP averages were removed at each electrode site, ΔVEP waveshape pairs for the form (Fig. 2, column 3) axis and the color (Fig. 2, column 4) axis were nearly identical and 180° out of phase. In contrast, ΔVEP waveshape pairs for the orthogonal axes (Fig. 2, column 5: form vs. color) were effectively uncorrelated. The sign and magnitude of the squared correlation coefficients (r^2) for each pair of ΔVEP waveshapes is presented to the left of the tracings for each recording location and axis comparison (form, color, and orthogonal). Each VEP and ΔVEP waveshape was based on averages from eight subjects, and contained $N \approx 740$ waveforms (i.e., stimulus presentations). Each waveshape pair is composed of dotted and solid line tracings that identify primary attributes named in each figure heading (columns 3–5). In all cases, the first named attribute is the dotted line, and the second named attribute is the solid line. The epoch length of each waveshape was 500 msec, using 100 points with 5 msec/point resolution. The amplitude of all VEP waveshapes was equated by transformation to a z-score scale with a Mean = 0, and σ = 1.0. The maximum peak-to-peak amplitude of VEP waveshapes varied, over the scalp, from $Z = \pm 2.61$ to $Z = \pm 2.98$. The maximum peak-to-peak amplitude of ΔVEP waveshapes varied, over the scalp, from $Z = \pm 1.16$ to $Z = \pm 1.53$. Please note that the Scaling factor for ΔVEP waveshapes is 50% larger than that for VEP waveshapes.

values. Please note that for the orthogonal axis, form waveshapes were computed as the average of the circle and (sign inverted) triangle ΔVEPs, and color waveshapes were computed as the average of the green and (sign inverted) red ΔVEPs.

As can be seen, the unit circle model (e.g., AS) predicted ΔVEP waveshape pairs with considerable accuracy. Figure 2, column 3, shows that ΔVEP waveshape pairs for the form axis (circle vs. triangle) were nearly identical (r^2 = 95–99%) and 180° out of phase. Similarly, Fig. 2, column 4, shows that the ΔVEP waveshapes for the color axis (green vs. red) were also similar (r^2 = 44–93%) and 180° out of phase. Finally, Fig. 2, column 5, shows that the ΔVEP waveshape pairs on orthogonal axes were effectively unrelated (r^2 = 0–20%). An inspection of all subject ΔVEPs revealed the same findings, and Table 1 provides a summary of the r^2 values for each subject, electrode, primary axis; i.e., form, color, and orthogonal. The data presented in Table 1 show that all of the subjects exhibited the same ΔVEP waveshape pair relationships as the GROUP averages presented in Fig. 2, columns 3–5.

Since the CATEGORIZED ΔVEP waveshape pairs provided such strong evidence that the waveshapes contained stable classification components for form and color information, a complementary hypothesis was advanced to determine whether the robust ΔVEP classification symmetries could be broken by randomizing subject VEP waveshapes produced by visual stimulation and then recompute the marginal averages, EVEP and ΔVEP waveshapes, as before. It followed, therefore, that if RANDOMIZED VEP waveshapes produce ΔVEPs that have little, or no, classification information, it would seem safe to conclude that the original CATEGORIZED waveshapes contained stable classification information. The complementary hypothesis was tested by: (1) randomly assigning each subject's VEPs for green circle, green triangle, red circle, and red triangle to the cells (C1F1, C1F2, C2F1, C2F2) of the stimulus matrix. The randomization was constrained so that, with four stimuli for each of eight subjects, the new cell VEP averages contained two waveshapes for each stimulus in the set; (2) recalculating the primary marginal (i.e., F1, circle; F2, triangle; C1, green; C2, red) VEP waveshapes; (3) recalculating the EVEP averages (CF); and then (4) recalculating the ΔVEP waveshape pairs.

The RANDOMIZED EVEP (same as EVEP for CATEGORIZED data), VEP and ΔVEP waveshapes shown in Fig. 3 provided decidedly different results than those obtained with CATEGORIZED waveshapes. It can be seen that the input of randomized VEP waveshapes clearly degraded the strong polar symmetries (180° phase-reversal) observed with CATEGORIZED waveshapes. Whereas a few brain regions exhibit moderate r^2 values, on the average, r^2 values for RANDOMIZED ΔVEP waveshape pairs were 75.9% lower than CATEGORIZED ΔVEPs on the

TABLE 1
Squared-Correlations for ΔVEP Waveshape Pairs (r^2 = %)

Ss	C3	C4	T5	T6	P3	P4	O1	O2	Sm
				(A) Form axis (circle vs. triangle)					
S1	−82	−99	−99	−99	−96	−99	−97	−98	−96
S2	−85	−88	−99	−99	−99	−99	−99	−94	−95
S3	−94	−99	−99	−99	−99	−99	−99	−99	−98
S4	−92	−96	−99	−99	−97	−98	−98	−99	−97
S5	−99	−99	−97	−99	−99	−99	−98	−99	−98
S6	−83	−98	−99	−99	−94	−97	−99	−99	−96
S7	−97	−98	−93	−99	−97	−98	−98	−99	−97
S8	−99	−99	−99	−99	−99	−99	−99	−99	−99
Em	−91	−97	−98	−99	−97	−98	−98	−98	−97
				(B) Color axis (green vs. red)					
S1	−99	−99	−99	−75	−87	−99	−63	−58	−84
S2	−89	−88	−99	−87	−99	−99	−99	−97	−94
S3	−95	−99	−99	−99	−99	−99	−77	−57	−90
S4	−97	−93	−81	−74	−87	−85	−58	−49	−78
S5	−99	−99	−93	−99	−99	−99	−85	−99	−96
S6	−99	−87	−99	−99	−97	−93	−99	−99	−96
S7	−88	−66	−92	−71	−91	−88	−91	−99	−86
S8	−87	−99	−99	−99	−99	−99	−99	−85	−96
Em	−94	−91	−95	−88	−94	−95	−84	−80	−90
				(C) Orthogonal axes (form vs. color)					
S1	−1	0	−7	−22	−4	−4	−12	−19	8
S2	0	−4	−2	2	0	1	8	13	4
S3	−19	−3	−6	−9	0	0	1	0	4
S4	−10	−2	0	−2	−2	−1	0	0	2
S5	0	0	18	0	2	0	5	4	4
S6	2	0	−3	0	6	2	3	7	2
S7	−36	0	0	−10	−5	−1	3	0	6
S8	−33	−2	2	−1	−4	0	14	0	7
Em	12	1	4	6	4	1	6	5	5

Note. Ss(S1–S8), subjects; Em, electrode means; Sm, subject means.

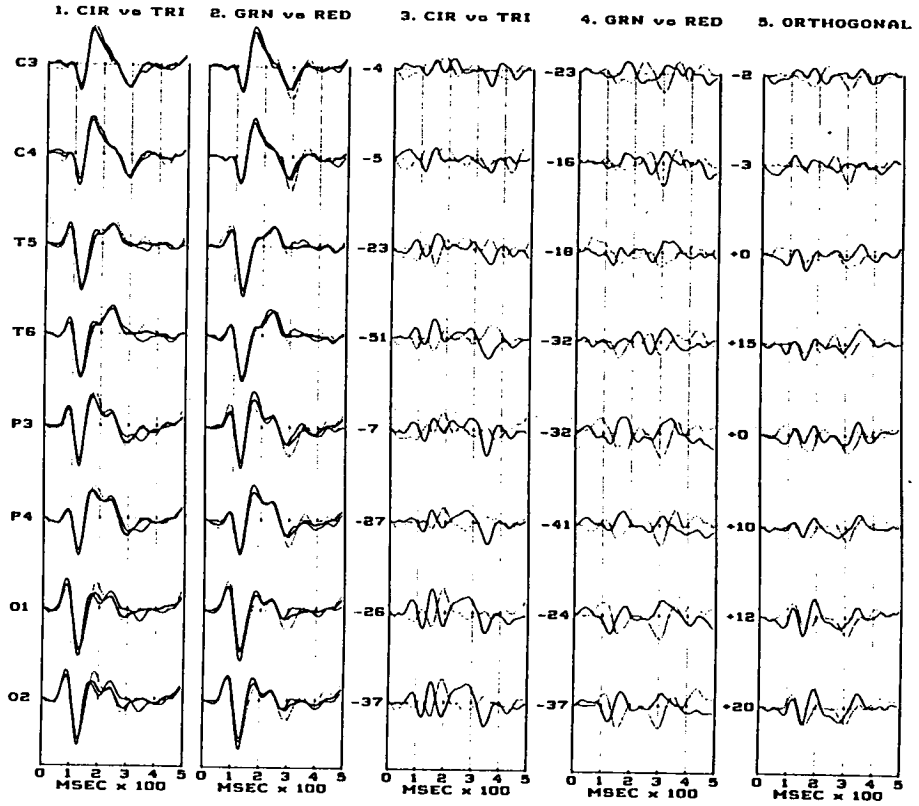

FIG. 3. Depiction of RANDOMIZED VEP waveshapes and ΔVEP waveshape pairs for the GROUP mean (MN). Column 1 depicts the averaged EVEP waveshape for each electrode (thick line) along with the form (circle vs. triangle) VEP waveshapes, that do not deviate symmetrically around their respective EVEP averages. Column 2 presents the EVEP waveshapes for each electrode (thick line) along with the color (green vs. red) VEP waveshapes, that also do not deviate symmetrically around the EVEP average. Column 3 depicts the ΔVEP waveshape pairs for the form (circle vs. triangle) axis that do not have the same waveshapes. Column 4 shows the ΔVEP waveshape pairs for the color (green vs. red) axis that also do not have the same waveshapes. Column 5 presents ΔVEP waveshape pairs for the orthogonal axes (form vs. color). The sign and magnitude of the squared correlation coefficients (r^2) is shown next to each ΔVEP waveshape pair. The parameters, data tracings, and scaling factors are the same as those reported in Fig. 2.

form axis (circle vs. triangle), and 48.0% lower than CATEGORIZED ΔVEPs on the color axis (green vs. red). There were no differences between r^2 values for RANDOMIZED and CATEGORIZED ΔVEP waveshape pairs on ORTHOGONAL axes. These findings clearly show that RANDOMIZED ΔVEP waveshape pairs do not contain classification information. Therefore, the CATEGORIZED findings appear to be robust because they do contain stable form and color waveshape components.

An analysis of the CATEGORIZED data showed that (a) there was no overall difference in ΔVEP waveshape pair r^2 values obtained from different electrodes ($F(7, 56) = 0.95$, $p = 0.48$); (b) there were substantial differences among r^2 values for ΔVEP waveshape pairs on the form, color, and orthogonal axes ($F(1, 56) = 2380.96$, $p_{HF} = 0.0009$). A single degree-of-freedom polynomial contrast showed that there were no differences between r^2 values for waveshape pairs on the form and color axes and that these values were significantly higher than the r^2 values on the orthogonal axes ($F(8, 56) = 656.40$, $p = 0.0009$); (c) the r^2 values for ΔVEP waveshape pairs on the form, color, and orthogonal axes depended

TABLE 3
Anatomical Distribution of Transfer Functions

(A) Squared correlations between PS and AS vectors (r^2 = %)

Ss	C3	C4	T5	T6	P3	P4	O1	O2	Sm
S1	98	99	99	99	99	99	98	98	98
S2	99	99	99	99	99	99	99	99	99
S3	99	99	99	98	99	99	99	98	99
S4	99	99	99	99	99	99	99	99	99
S5	99	99	99	99	99	99	99	99	99
S6	98	99	99	99	99	99	99	99	99
S7	98	99	99	98	99	99	99	99	99
S8	98	98	99	99	99	99	99	99	99
Em	98	99	99	99	99	99	99	99	99

(B) Distribution of PS errors (PS°–AS°)

AS°	C3	C4	T5	T6	P3	P4	O1	O2	Am
0	0	0	0	0	0	0	0	0	0
45	−10	−14	−8	−18	−13	−12	−18	−18	−14
90	9	2	1	8	4	0	−8	−4	2
135	1	1	−2	12	−1	2	−1	4	2
180	−1	−1	−0	−0	0	−1	2	1	0
225	11	4	−1	−4	7	0	2	−0	2
270	12	3	2	10	4	3	−5	−1	4
315	16	16	10	17	10	11	10	9	12
Em	5	2	0	4	2	1	−2	−1	1

Note. Ss(S1–S8), subjects; Em, electrode mean; Sm, subject mean; Am, Angular mean.

analysis of these data showed the following: (a) There were no differences in the distribution of errors among electrodes ($F(7, 56) = 1.00, p = 0.44$). (b) The average distribution of errors differed significantly within the stimulus set ($F(6, 336) = 46.95$; $p_{HF} = 0.0009$). Single degree-of-freedom contrasts showed that these differences were primarily due to the fact that the ΔVEPs for the circle stimuli (i.e., green and red circles) were less influenced by color variations and, consequently, were mislocated 13° closer to the circle, positioned at 0° (green: $F(1, 56) = 141.35$, $p = 0.0009$; red: $F(1, 56) = 68.49$, $p = 0.0009$). (c) The angular error in positioning each of the eight ΔVEPs did not depend upon specific electrode locations ($F(42, 336) = 1.32$, $p_{HF} = 0.15$).

DISCUSSION

We can now return to the original questions posed in this paper. Recordings of VEP waveshapes were obtained from human observers during visual stimulation with an abstract stimulus set, an AS. The PS indices extracted from the ΔVEP waveshapes reflected an abstract interpretation of the AS with very high accuracy. These results provide substantial evidence that the abstract content of human visual processing can, within certain limitations, be identified in VEP waveshape recordings. Insofar as the transfer functions, PS = AS, were consistent with an abstract classification, absolute sensory and perceptual attributes were clearly not evident. Therefore, the specificity of ΔVEP waveshapes for the attributes of the stimuli were *relative* to the present set of stimuli.

Although the results for individual subjects were robust, this does not mean that every subject had the same VEP waveshapes. To the contrary, these and other studies show that, with complex stimuli, the VEP waveshape exhibits the properties of other biological markers for subject identity (e.g., voice print, fingerprint, eye print, DNA): (a) everyone has VEP waveshapes; (b) there appear to be nominally distinct families of the VEP waveshape pattern with, perhaps, predictable incidence rates in the population; and (c) in the end, the actual VEP waveshape is unique for the individual. Therefore, Tables 1–3 provide the essential evidence that the results (i.e., waveshape pair correlations, signal strength indices, and transfer functions) were not only reliable across subjects, these data also show that the results were somewhat more robust for within-subject calculations.

The primary hypothesis predicted that the obtained VEP waveshapes would be a linear composite of N orthogonal waveshape components that were required to account for the N-dimensional AS (orthogonal stimulus matrix) presented to the subjects. The a priori model (i.e., Fig. 1B) provided an abstract (conceptual) interpretation of the AS vector that required only two bipolar dimensions. Transfer functions that were returned in ΔVEP PS vectors provided several challenging conclusions. (a) Eighty-six to ninety percent of the variance in ΔVEP data sets ($n = 8$ waveshapes) could be attributed to two bipolar dimensions (i.e., varimax components), having the same configuration as the AS model. These findings provided excellent support for the primary hypothesis. (b) Ten to fourteen percent of the variance in ΔVEP data sets was due to unknown sources of error. (c) The exogenous EVEP waveshape component, which was removed from VEP data sets, constituted an additional VEP waveshape component and suggests that the primary hypothesis should be modified to reflect this source of variability. Therefore, the primary hypothesis can be restated: *The VEP waveshape is a linear product space, composed of N + 1 orthogonal waveshape components (and error variance) which are requisite in number to span an N-dimensional attribute space and a single observer dimension (i.e., experimental intrusion).*

The most fascinating finding in these studies was the fact that the AS model predicted major ΔVEP waveshape phase relationships. While varimax components analysis was only used to quantify these relationships

TABLE 2
ΔVEP Waveshape Signal Strength Index (Z)

Ss	C3	C4	T5	T6	P3	P4	O1	O2	Sm
				(A) Form VEPs					
S1	18.0	21.2	55.0	59.4	43.8	42.7	55.5	57.2	44.0
S2	44.5	38.4	33.5	30.2	33.4	22.8	23.6	25.5	31.4
S3	26.7	25.5	38.2	43.0	47.4	49.0	47.2	49.4	40.8
S4	23.2	27.0	53.1	45.8	45.3	42.9	56.8	53.4	43.4
S5	29.4	32.1	30.0	30.7	34.3	28.9	39.3	36.5	32.6
S6	17.4	28.8	20.6	35.3	21.9	27.2	25.9	29.7	25.8
S7	39.1	43.4	32.8	39.2	37.1	34.7	29.0	34.0	36.1
S8	40.2	46.5	29.0	29.5	29.8	23.7	15.2	23.6	29.6
Em	29.8	32.9	36.5	39.1	36.6	35.2	36.6	38.7	35.7
				(B) Color VEPs					
S1	29.2	27.2	42.1	44.3	38.5	34.6	40.9	40.4	37.1
S2	46.0	38.3	24.7	20.9	34.0	25.8	28.5	29.1	30.9
S3	27.7	26.0	26.5	20.8	30.3	26.0	32.2	27.5	27.1
S4	27.2	25.1	42.3	31.6	37.7	33.8	41.8	35.0	34.3
S5	23.7	22.7	25.9	26.9	27.3	26.3	30.5	25.3	26.0
S6	27.2	20.7	23.7	19.6	24.1	23.6	25.5	28.3	24.0
S7	32.5	29.1	33.0	23.3	33.1	28.2	23.3	25.4	28.4
S8	30.2	24.2	34.0	23.7	33.6	26.6	15.8	26.7	26.8
Em	30.5	26.7	31.7	26.4	32.3	28.1	29.8	29.7	29.4

Note. Ss(S1–S8), subjects; Em, electrode means; Sm, subject means.

upon specific electrode locations ($F(14, 112) = 2.38$, $p_{HF} = 0.006$). This finding was primarily due to the fact that the left central electrode (C3) provided significantly lower r^2 values for the form axis and slightly higher r^2 values for the orthogonal axes. The reliability of these findings for individual subjects can be verified by the results presented in Table 1.

Evaluation of VEP signal strength. Table 2 presents signal strength indices for the form (A) and color (B) ΔVEP waveshapes obtained from each subject (S1–S8) and electrode derivation (C3–O2). As can be seen in Table 2, the signal strength of form ΔVEPs was generally larger than color ΔVEPs. An analysis of these data showed that (a) there were no differences in ΔVEP signal strength among different electrodes ($F(7, 56) = 0.39$, $p = 0.90$), (b) the signal strength of form ΔVEP waveshapes was significantly larger than that of color ΔVEP waveshapes ($F(1, 56) = 41.68$; $p = 0.0009$), and (c) there was marginal evidence that form and color ΔVEP signal strength indices depended upon specific electrode locations ($F(7, 56) = 1.93$; $p = 0.08$). However, these could not be verified with multiple comparisons tests.

Evaluation of transfer function. Figure 4A presents the observed GROUP PS vectors for each electrode derivation. As can be seen, these

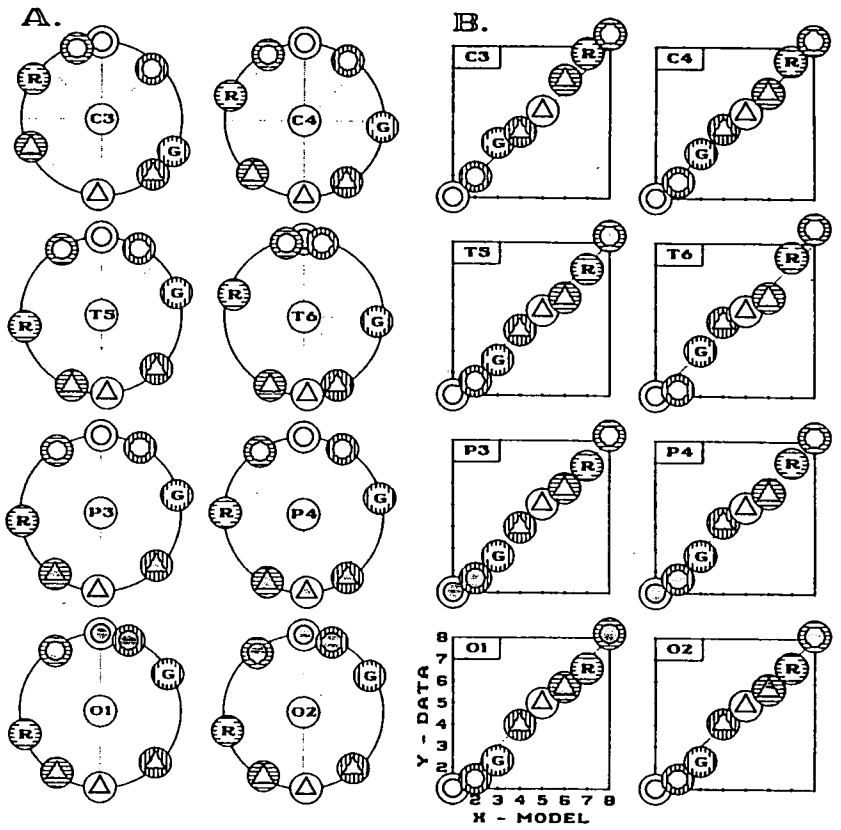

FIG. 4. Graphic analysis of the transfer function, AS = PS, for each electrode location. Observed output PS vectors for each electrode location. These results show how well the observed ΔVEP data sets reproduce the unit circle classification. (B) Scattergrams based upon the expected, AS, vector (MODEL = x axis) and the averaged observed, PS, vectors (DATA = y axis). The statistical analyses for these data are presented in text, and the specific values can be found in Tables 3A and 3B. Circle, triangle, green, and red features are represented by the same graphic coding scheme as that described for Fig. 1.

findings closely approximate the unit circle model specified in the AS vector. Figure 4B provides a scatterplot for each electrode, in which the AS and PS vectors are graphed on the X (MODEL) and Y (DATA) axes, respectively. Nonparametric and parametric correlations between the AS and the 72 observed PS vectors ranged from 0.98 to 1.0, to yield an average predictability of 99%. Table 3A shows that the quality (r^2) of observed transfer functions was reliable across subjects and electrodes.

Table 3B presents the average deviations (i.e., angular error) from the expected position of the eight ΔVEPs on the octants of the unit circle. As can be seen, the average error for all electrodes and subjects was only 1°. However, there were systematic errors which require discussion. An

in PS vectors, there can be little doubt that the averaged ΔVEP waveshapes (Fig. 2) directly exhibited all of the properties predicted by the AS model. Where the model defined stimulus features as opposing poles of an attribute dimension (i.e., form *or* color), ΔVEP waveshapes were nearly identical and 180° out of phase. Similarly, where the model defined form *and* color attributes on orthogonal axes (i.e., *x*, *y*), ΔVEP waveshapes for the form and color axes were effectively uncorrelated (average $r^2 = 5\%$).

These results provided strong evidence that the original VEP waveshapes contained valid form and color classification information. To validate these findings further, a complimentary hypothesis posed that if the original VEP waveshapes contained valid form and color classification information, then the entire classification could be broken by reconstructing the ΔVEP waveshapes from a RANDOMIZED set of VEP waveshapes that included exemplars for every stimulus in the set. This analysis revealed sets of *random* ΔVEP waveshapes that had little or no form and color classification information. Therefore, the primary hypothesis, and the derived AS model, appear to accurately reflect the allocation of VEP waveshape resources (PS) when human observers view stimuli that constitute an abstract classification.[1]

The present results raise a number of provocative questions concerning the organization of neuronal generator systems that can exhibit the VEP waveshape dynamics observed in this work. Specifically, the averaged EVEP and ΔVEP waveshapes shown in Fig. 2 lead directly to the inference that the underlying neuronal system(s) *use* phase-encoded eigenfunctions to represent the abstract classification. The significance of this coding (representational) scheme becomes evident when the possible neural origins of EVEP and ΔVEP waveshape components are considered. Nunez (1981) provides a detailed account of the neurophysical bases for different wave phenomena in the central nervous system, and the calculations that are required to define such wave phenomena are extensive, nontrivial, and obviously not carried out in the current studies. However, the observed behavior of the EVEP and ΔVEP waveshapes suggest the hypothesis that these waveshape components could reflect *propagated* and *standing* waves, respectively, that arise from distinct anatomical compartments (Nunez, 1981, pp. 315–346).

For example, the observed EVEP waveshapes are analogous to propagated waves that occur when information is transmitted through the pathways and associated nuclei of the retino–striate system. The successive peaks of the VEP waveshape are typically associated with activation of each of the neuronal links associated with the retino–striate system and, thus, the analogy makes partial sense.

Similarly, the observed behavior of ΔVEP waveshapes are analogous to cortical standing waves, in which propagated waves are mapped into the visual cortex where the cortical architecture is organized as a sheet of dipole columns that are interlaced with interneurons and horizontal fibers. The consequence of this horizontal organization enables cortical architectures to support standing waves that entail the algebraic sum of *N* orthogonal waveshapes (i.e., eigenfunctions) which are sufficient in number to match *N* input stimuli (adapted from Nunez, 1981). While this part of the analogy also seems to be consistent with the observed behavior of ΔVEP waveshapes, the author would point to two additional properties that are not currently part of the standing wave model. First, the standing wave model employs eigenfunctions for the algebraic summation of *successive* input stimuli. The current studies show that the cortex also supports *simultaneous* eigenfunctions that reflect conjoined stimulus attributes. Second, the standing wave model does not currently support the influence of experience and learning, by which a myriad of distinct stimuli (or attributes) attain abstract equivalences that simplify (reduce dimensionality) the organization, plasticity, and recall of cognitive representations. These revisions entail the operational definitions for AS and PS, as exemplified in the primary hypothesis used here.

During the period this paper was in the review process, Young and Yamane (1992) have shown that the discharge pattern of neuronal populations in monkey inferotemporal cortex encode human faces ($n = 27$ photographs) in two dimensions that served to identify specific individuals (i.e., laboratory personnel), based upon the configuration of facial attributes. They used analytic methods similar to those presented in the cur-

[1] The impression has been voiced that the findings obtained in this study may be due to linear calculation dependencies that inevitably lead to artifactual robustness. This impression arises from attempts to decompose the complexity of the entire VEP classification into simpler operations, for example, calculating ΔVEP waveshapes for one axis at a time. From this perspective, constraining the analysis to two VEP waveshapes, the mean of *any pair* of VEP waveshapes is centered within the range of the waveshape pair, and the ΔVEP waveshapes will deviate symmetrically around *their* mean. Then, if successive axes (pairs of VEP waveshapes) are examined in turn, each ΔVEP waveshape pair will deviate symmetrically around *their* mean. Finally, this view concludes that, if the above were true, then a completely *random* set of VEP waveshape patterns would *always* yield perfect ΔVEP classifications. This simplified interpretation misrepresents the procedures used in the present studies. The present procedures were based upon eight VEP waveshapes, and to achieve the ΔVEP classifications reported here, the EVEPs were centered *between all eight VEP waveshapes simultaneously*. As soon as four or more VEP waveshapes are entered into the analysis, artifactual classifications cannot be found. ΔVEP classifications only emerge if they exist in the original input VEP waveshapes. For example, calculate the mean (i.e., EVEP) for any four values, using a two-dimensional approach with two axes and two values/axis. The computed deviation scores are *always* symmetrical around EVEP when the *four input* values are symmetrical (i.e., classified input: $x = (5, 15)$, $y = (5, 15)$; mean = 10; and output: $x = (-5, +5)$, $y = (-5, +5)$), but the computed deviation scores are *never* symmetrical around the mean when the *four input* values are asymmetrical (i.e., unclassified input: $x = (5, 15)$, $y = (10, 15)$; Mean = 11.25; and output: $x = (-6.25, +3.75)$, $y = (-1.25, +3.75)$).

rent paper, and they concluded that facial classifications were based upon a sparse (i.e., distributed) population code. Since the discharge pattern of neuronal populations is determined by the algebraic sum of dendritic slow potentials, it seems likely that their findings may also entail phase-encoded eigenfunctions that reveal phase reversals for the polar endpoints of two facial attribute dimensions. Obviously, the accuracy of this inference requires empirical validation.

The results obtained in the current studies, and in the findings of Young and Yamane (1992), are based upon the method of conjoint similarities and differences. As Young and Yamane observe, this method provides stronger hypothesis-testing strategies than traditional methods. In the current studies, for example, it can be seen that the use of orthogonalized stimulus attributes (i.e., AS) and structural analysis clearly obviate alternative interpretations (e.g., differences in attention or arousal) that have previously been offered to exclude perceptual or cognitive interpretations of VEP data. It seems likely that this method can provide robust predictions and tests of hypotheses concerning cerebral processes that underlie a number of specific psychological processes. Thus, in the present work, the method tends to increase the certainty that cerebral mechanisms are engaged in *cognitive work*, rather than support functions.

As a concluding question: What do the present findings reveal about the brain mechanisms of cognitive function, especially with regard to conceptual classifications? The results have addressed two fundamental issues. First, the results imply that the underlying neural generator system has, at minimum, the functional capacities of a cortical sheet, and it seems likely that these correspond to traditional cortical systems. Second, the results also implied that the underlying neural generator system used phase-encoded eigenfunctions to represent an abstract classification. These two observations lead to the conclusion that the relevant cortical systems can be understood from the perspectives of *computational anatomy* (Hudspeth, 1985, 1990; Hudspeth, 1993; Hudspeth & Pribram, 1990, 1992; John & Schwartz, 1978; Pribram, 1991; Schwartz, 1980, 1990). Assuming that such a model operated in the present instance, the author would have to conclude that product spaces are represented by computational systems and that the observed ΔVEP waveshape changes merely provided the inferences concerning the nature of cortical computation.

REFERENCES

Beglieter, H., & Porjesz, B. 1975. Evoked brain potentials as indicators of decision making. *Science*, **187**, 754–755.

Begleiter, H., Porjesz, B., & Garozzo, R. 1979. Visual evoked potentials and affective ratings of semantic stimuli. In: H. Begleiter (Ed.), *Evoked brain potentials and behavior*. New York: Plenum.

Buchsbaum, M., Coppola, R., & Bittker, T. E. 1974. Differential effects of congruence, stimulus meaning and information on early and late components of the averaged evoked response. *Neuropsychologia*, **12**, 533–545.

Chapman, R. M. 1977. Methods of evoked potentials analysis in linguistic research. In: D. A. Otto (Ed.), *Multidisciplinary perspectives in event-related potential research*. Washington, DC: Government Printing Office.

Chapman, R. M., McCrary, J. W., Chapman, J. A., & Bragdon, H. R. 1978. Brain responses related to semantic meaning. *Brain and Language*, **5**, 195–205.

Degerman, R. L. 1972. The geometric representation of some simple structures. In: R. N. Shepard, A. K. Romney, and S. B. Nerlove (Eds.), *Multidimensional scaling: Theory and applications in the behavioral sciences*. New York: Seminar Press.

Graham, C. H. 1960. Visual perception. In: S. S. Stevens (ed.), *Handbook of experimental psychology*. New York: Wiley.

Guttman, L. 1954. A new approach to factor analysis: The radex. In: P. F. Lazarsfield (Ed.), *Mathematical thinking in the social sciences*. Glencoe, IL: Free Press.

Guertin, W. H., & Bailey, J. P., Jr. 1970. *Introduction to modern factor analysis*. Ann Arbor: Edwards Brothers.

Hillyard, S. A., Picton, T. W., & Regan, D. 1978. Sensation, perception and attention: Analysis using ERPs. In: *Event-related brain potentials in man*. E. Callaway, P. Tueting, & S. H. Koslow (Eds.), New York: Academic Press.

Hillyard, S. A., & Picton, W. T. 1979. Event-related brain potentials and selective information processing in man. In: J. E. Desmedt (Ed.), *Progress in clinical neurophysiology, cognitive components in cerebral event-related potentials and selective attention*. Basel: Karger. Vol. 6.

Hudspeth, W. J., & Jones, G. B. 1977. Neural models for short-term memory: A quantitative study of averaged evoked potential waveform. *Neuropsychologia*, **16**, 201–212.

Hudspeth, W. J. 1985. Developmental neuropsychology: Functional implications of quantitative EEG maturation. *Journal of Clinical and Experimental Neuropsychology*, **7**, 606. [Abstract]

Hudspeth, W. J. 1990. VEPs and dimensions of visual perception. *Proceedings of the Fifth International Congress of Psychophysiology*, 132. [Abstract]

Hudspeth, W. J. 1993. Knowledge representation in brain electrical activity. In: D. S. Levine and M. Aparicio (Eds.), *Neural Networks for Knowledge Representation and Inference*. Hillsdale, NJ: Lawrence Erlbaum Associates. In press.

Hudspeth, W. J., & Pribram, K. H. 1990. Stages of brain and cognitive maturation. *Journal of Educational Psychology*, **82**, 880–883.

Hudspeth, W. J., & Pribram, K. H. 1992. Psychophysiological indices of cerebral maturation. *International Journal of Psychophysiology*, **12**, 19–29.

Jasper, H. H. 1958. The ten–twenty electrode system of the International Federation. *Electroencephalography and Clinical Neurophysiology*, **10**, 371–375.

John, E. R., Herrington, R. N., & Sutton, S. 1967. Effects of visual form on the evoked response. *Science*, **155**, 1439–1442.

John, E. R., Walker, P., Cawood, D., Rush, M., & Gehrmann, J. 1972. Mathematical identification of brain states applied to classification of drugs. *International Review of Neurobiology*, **15**, 273–347.

John, E. R. 1977. *Functional neuroscience: Neurometrics: Clinical applications of quantitative neurophysiology*. Hillsdale, NJ: Erlbaum. Vol. 2.

John, E. R., & Schwartz, E. L. 1978. The neurophysiology of information processing and cognition. *Annual Review of Psychology*, **29**, 1–29.

Johnston, V. L., & Chesney, G. L. 1974. Electrophysiological correlates of meaning. *Science*, **186**, 944–946.

Künnapas, T. Mälhammar, G., & Svenson, O. 1964. Multidimensional ratio scaling and

multidimensional similarity of simple geometric figures. *Scandanavian Journal of Psychology*, **5**, 249–256.

Nunez, P. L. 1981. *Electrical fields of the brain: Neurophysics of EEG*. New York: Oxford Univ. Press.

Rapoport, A., & Fillenbaum, S. 1972. An experimental study of semantic structure. In: A. K. Romney, R. N. Shepard, & S. B. Nerlove (Eds.), *Multidimensional scaling: Theory and applications in the behavioral sciences*. New York: Seminar Press. Vol. 2.

Pribram, K. H. 1991. *Brain and perception: Holonomy and structure in figural processing*. Hillsdale, NJ. Erlbaum.

Regan, D. 1972. *Evoked potentials in psychology, sensory physiology and clinical medicine*. New York: Wiley–Interscience.

Roemer, R. A., & Teyler, T. J. 1977. Auditory evoked potential asymmetries related to word meaning. In: J. Desmedt (Ed.), *Progress in clinical neurophysiology: Language and hemispheric specialization in man: Cerebral event-related potentials*. Basel: Karger. Vol. 3.

Schwartz, E. L. 1980. Computational anatomy and functional architecture of striate cortex: A spatial mapping approach to perceptual coding. *Vision Research*, **20**, 645–669.

Schwartz, E. L. 1990. *Computational neuroscience*. Cambridge: MIT–Bradford Press.

Shelburne, S. A., Jr. 1973. Visual evoked response to language stimuli in children with reading disabilities. *Electroencephalography and Clinical Neurophysiology*, **34**, 135–143.

Shepard, R. N. 1972. The taxonomy of some principal types of data and multidimensional methods for their analysis. In: R. N. Shepard, A. K. Romney, & S. B. Nerlove (Eds.), *Multidimensional scaling: Theory and applications in the behavioral sciences*. New York: Seminar Press.

Thatcher, R. W. 1977a. Evoked potential correlates of delayed letter matching. *Behavioral Biology*, **19**, 1–23.

Thatcher, R. W. 1977b. Evoked potential correlates of hemispheric lateralization during semantic information processing. In: S. Harnand, R. W. Doty, L. Goldstein, J. Jaynes, & G. Krauthamer (Eds.), *Lateralization of the nervous system*. New York: Academic Press.

Tyler, T. J., Roemer, R. A., Harrison, T. F., & Thompson, R. F. 1973. Human scalp recorded evoked-potential correlates of linguistic stimuli. *Bulletin of the Psychonomic Society*, **1**, 333–334.

Wilkenson, L. 1990. *Systat: The system for statistics (Ver. 5.0)*. Evanston, IL: Systat, Inc.

Young, M. P., & Yamane, S. 1992. Sparse population coding of faces in the inferotemporal cortex. *Science*, **256**, 1327–1331.

NLP 139a

RANDOMIZATION CONTROLS FOR THE LINEAR DEPENDENCE HYPOTHESIS

For Manuscript (COGG061):
BRAIN ELECTRICAL ACTIVITY: I. FORM AND COLOR CLASSIFICATION

William J. Hudspeth
Center for Brain Research
Radford University
Radford, VA 24142

		INPUT	ΔOUT
COLOR	X1:	5	-2.50
	X2:	10	2.50
FORM	Y1:	5	-2.50
	Y2:	10	2.50
MEAN:		7.50	
ΔMAX:		2.50	

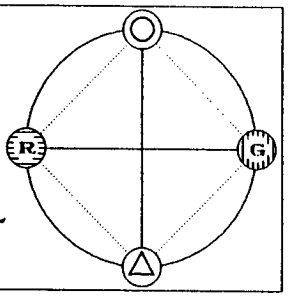

		INPUT	ΔOUT
COLOR	X1:	39	21.50
	X2:	4	-13.50
FORM	Y1:	9	-8.50
	Y2:	18	0.50
MEAN:		17.50	
ΔMAX:		21.50	

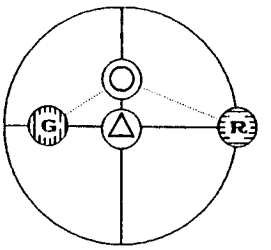

		INPUT	ΔOUT
COLOR	X1:	33	2.00
	X2:	43	12.00
FORM	Y1:	17	-14.00
	Y2:	31	0.00
MEAN:		31.00	
ΔMAX:		14.00	

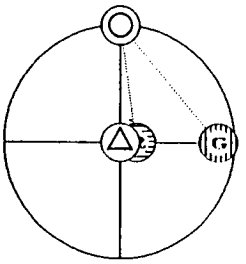

		INPUT	ΔOUT
COLOR	X1:	10	-7.75
	X2:	16	-1.75
FORM	Y1:	6	-11.75
	Y2:	39	21.25
MEAN:		17.75	
ΔMAX:		21.25	

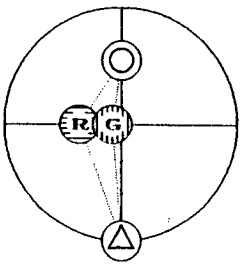

		INPUT	ΔOUT
COLOR	X1:	50	10.50
	X2:	42	2.50
FORM	Y1:	35	-4.50
	Y2:	31	-8.50
MEAN:		39.50	
ΔMAX:		10.50	

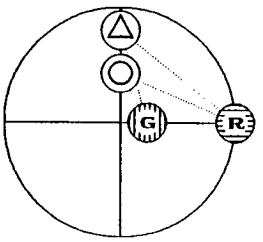

		INPUT	ΔOUT
COLOR	X1:	28	4.75
	X2:	16	-7.25
FORM	Y1:	5	-18.25
	Y2:	44	20.75
MEAN:		23.25	
ΔMAX:		20.75	

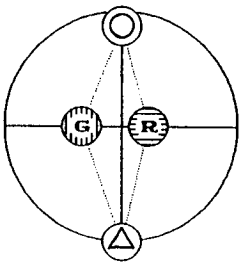

		INPUT	ΔOUT
COLOR	X1:	27	11.25
	X2:	5	-10.75
FORM	Y1:	9	-6.75
	Y2:	22	6.25
MEAN:		15.75	
ΔMAX:		11.25	

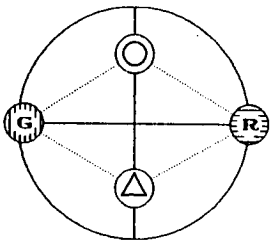

		INPUT	ΔOUT
COLOR	X1:	5	-11.50
	X2:	9	-7.50
FORM	Y1:	22	5.50
	Y2:	38	13.50
MEAN:		16.50	
ΔMAX:		13.50	

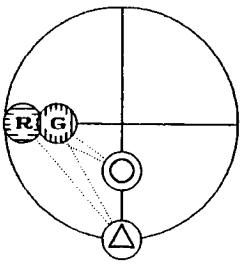

		INPUT	ΔOUT
COLOR	X1:	47	20.25
	X2:	15	-11.75
FORM	Y1:	29	2.25
	Y2:	16	-10.75
MEAN:		26.75	
ΔMAX:		20.25	

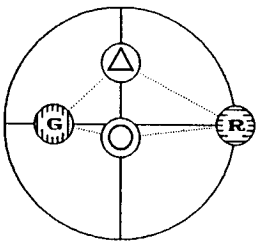

		INPUT	ΔOUT
COLOR	X1:	22	-6.00
	X2:	0	-20.00
FORM	Y1:	43	15.00
	Y2:	39	11.00
MEAN:		20.00	
ΔMAX:		20.00	

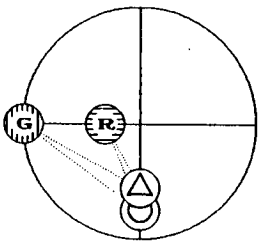

		INPUT	ΔOUT
COLOR	X1:	7	-23.00
	X2:	22	-8.00
FORM	Y1:	42	12.00
	Y2:	49	19.00
MEAN:		30.00	
ΔMAX:		23.00	

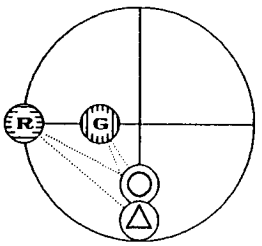

		INPUT	ΔOUT
COLOR	X1:	42	11.50
	X2:	14	-16.50
FORM	Y1:	17	-13.50
	Y2:	49	18.50
MEAN:		30.50	
ΔMAX:		18.50	

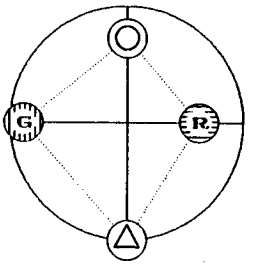

		INPUT	ΔOUT
COLOR	X1:	5	-2.50
	X2:	10	2.50
FORM	Y1:	5	-2.50
	Y2:	10	2.50
MEAN:		7.50	
ΔMAX:		2.50	

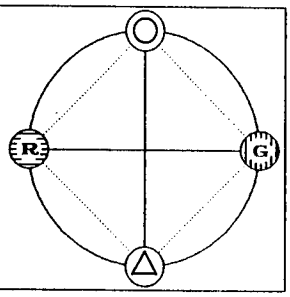

		INPUT	ΔOUT
COLOR	X1:	44	13.00
	X2:	48	17.00
FORM	Y1:	20	-11.00
	Y2:	12	-19.00
MEAN:		31.00	
ΔMAX:		19.00	

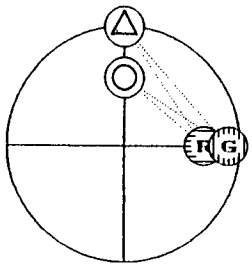

		INPUT	ΔOUT
COLOR	X1:	48	29.75
	X2:	11	-7.25
FORM	Y1:	10	-8.25
	Y2:	4	-14.25
MEAN:		18.25	
ΔMAX:		29.75	

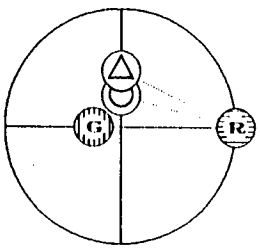

		INPUT	ΔOUT
COLOR	X1:	39	21.50
	X2:	4	-13.50
FORM	Y1:	9	-8.50
	Y2:	18	0.50
MEAN:		17.50	
ΔMAX:		21.50	

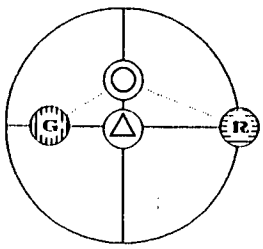

		INPUT	ΔOUT
COLOR	X1:	33	2.00
	X2:	43	12.00
FORM	Y1:	17	-14.00
	Y2:	31	0.00
MEAN:		31.00	
ΔMAX:		14.00	

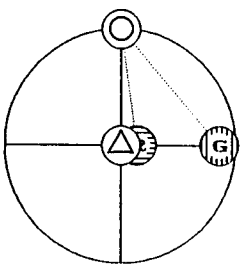

		INPUT	ΔOUT
COLOR	X1:	10	-7.75
	X2:	16	-1.75
FORM	Y1:	6	-11.75
	Y2:	39	21.25
MEAN:		17.75	
ΔMAX:		21.25	

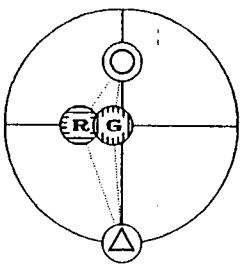

		INPUT	ΔOUT
COLOR	X1:	50	10.50
	X2:	42	2.50
FORM	Y1:	35	-4.50
	Y2:	31	-8.50
MEAN:		39.50	
ΔMAX:		10.50	

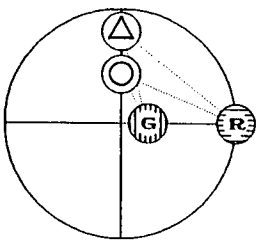

		INPUT	ΔOUT
COLOR	X1:	28	4.75
	X2:	16	-7.25
FORM	Y1:	5	-18.25
	Y2:	44	20.75
MEAN:		23.25	
ΔMAX:		20.75	

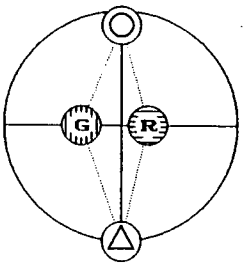

		INPUT	ΔOUT
COLOR	X1:	27	11.25
	X2:	5	-10.75
FORM	Y1:	9	-6.75
	Y2:	22	6.25
MEAN:		15.75	
ΔMAX:		11.25	

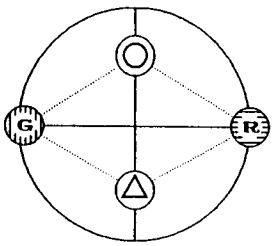

		INPUT	ΔOUT
COLOR	X1:	5	-11.50
	X2:	9	-7.50
FORM	Y1:	22	5.50
	Y2:	30	13.50
MEAN:		16.50	
ΔMAX:		13.50	

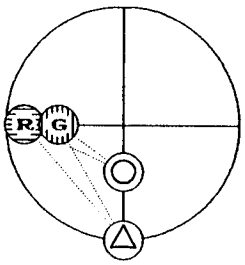

		INPUT	ΔOUT
COLOR	X1:	47	20.25
	X2:	15	-11.75
FORM	Y1:	29	2.25
	Y2:	16	-10.75
MEAN:		26.75	
ΔMAX:		20.25	

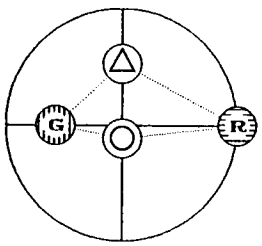

		INPUT	ΔOUT
COLOR	X1:	22	-6.00
	X2:	8	-20.00
FORM	Y1:	43	15.00
	Y2:	39	11.00
MEAN:		28.00	
ΔMAX:		20.00	

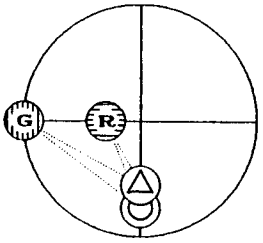

		INPUT	ΔOUT
COLOR	X1:	5	-2.50
	X2:	10	2.50
FORM	Y1:	5	-2.50
	Y2:	10	2.50
MEAN:		7.50	
ΔMAX:		2.50	

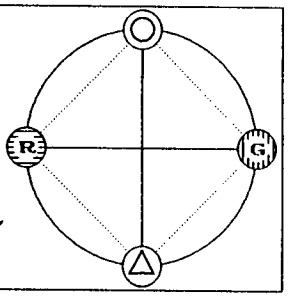

		INPUT	ΔOUT
COLOR	X1:	24	-2.75
	X2:	31	4.25
FORM	Y1:	34	7.25
	Y2:	10	-8.75
MEAN:		26.75	
ΔMAX:		8.75	

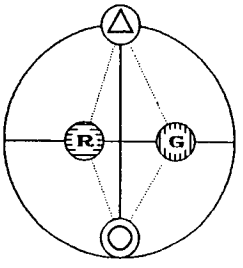

		INPUT	ΔOUT
COLOR	X1:	49	17.00
	X2:	28	-4.00
FORM	Y1:	9	-23.00
	Y2:	42	10.00
MEAN:		32.00	
ΔMAX:		23.00	

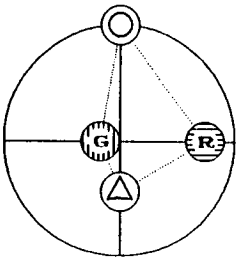

		INPUT	ΔOUT
COLOR	X1:	42	16.25
	X2:	35	9.25
FORM	Y1:	5	-20.75
	Y2:	21	-4.75
MEAN:		25.75	
ΔMAX:		20.75	

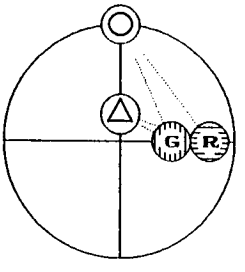

		INPUT	ΔOUT
COLOR	X1:	48	29.75
	X2:	11	-7.25
FORM	Y1:	10	-8.25
	Y2:	4	-14.25
MEAN:		18.25	
ΔMAX:		29.75	

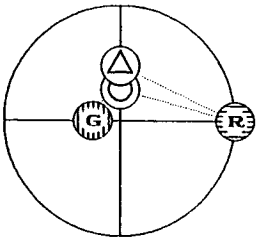

		INPUT	ΔOUT
COLOR	X1:	33	2.00
	X2:	43	12.00
FORM	Y1:	17	-14.00
	Y2:	31	0.00
MEAN:		31.00	
ΔMAX:		14.00	

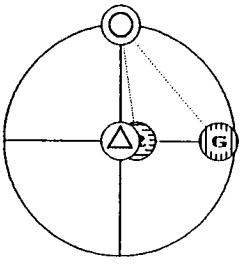

		INPUT	ΔOUT
COLOR	X1:	37	8.50
	X2:	1	-27.50
FORM	Y1:	44	15.50
	Y2:	32	3.50
MEAN:		28.50	
ΔMAX:		27.50	

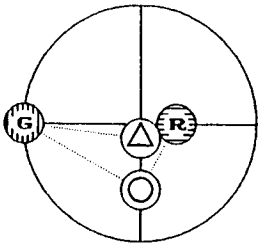

		INPUT	ΔOUT
COLOR	X1:	32	14.75
	X2:	6	-11.25
FORM	Y1:	23	5.75
	Y2:	8	-9.25
MEAN:		17.25	
ΔMAX:		14.75	

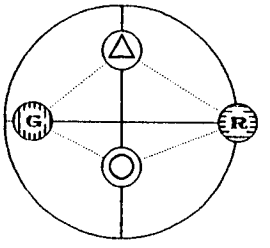

		INPUT	ΔOUT
COLOR	X1:	27	5.75
	X2:	12	-9.25
FORM	Y1:	22	0.75
	Y2:	24	2.75
MEAN:		21.25	
ΔMAX:		9.25	

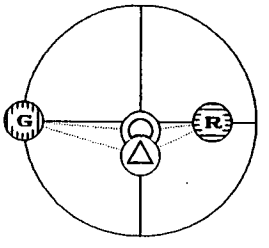

		INPUT	ΔOUT
COLOR	X1:	40	5.75
	X2:	10	-16.25
FORM	Y1:	29	-5.25
	Y2:	50	15.75
MEAN:		34.25	
ΔMAX:		16.25	

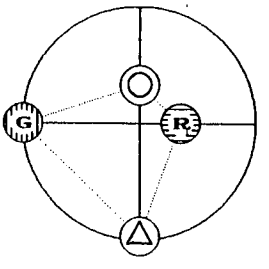

		INPUT	ΔOUT
COLOR	X1:	39	21.50
	X2:	4	-13.50
FORM	Y1:	9	-8.50
	Y2:	18	0.50
MEAN:		17.50	
ΔMAX:		21.50	

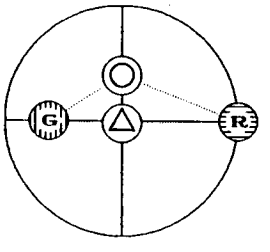

		INPUT	ΔOUT
COLOR	X1:	10	-7.75
	X2:	16	-1.75
FORM	Y1:	6	-11.75
	Y2:	39	21.25
MEAN:		17.75	
ΔMAX:		21.25	

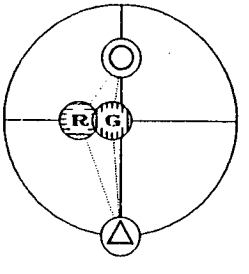

		INPUT	ΔOUT
COLOR	X1:	5	-2.50
	X2:	10	2.50
FORM	Y1:	5	-2.50
	Y2:	10	2.50
MEAN:		7.50	
ΔMAX:		2.50	

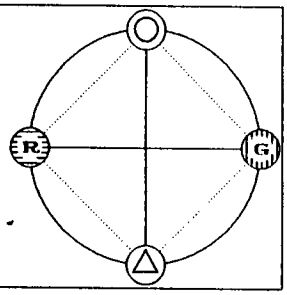

		INPUT	ΔOUT
COLOR	X1:	48	31.25
	X2:	2	-14.75
FORM	Y1:	7	-9.75
	Y2:	10	-6.75
MEAN:		16.75	
ΔMAX:		31.25	

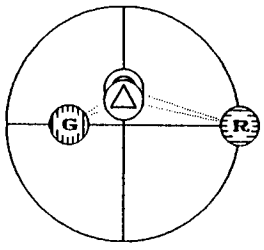

		INPUT	ΔOUT
COLOR	X1:	5	-11.50
	X2:	9	-7.50
FORM	Y1:	22	5.50
	Y2:	30	13.50
MEAN:		16.50	
ΔMAX:		13.50	

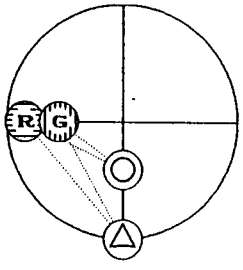

		INPUT	ΔOUT
COLOR	X1:	1	-8.25
	X2:	13	3.75
FORM	Y1:	2	-7.25
	Y2:	21	11.75
MEAN:		9.25	
ΔMAX:		11.75	

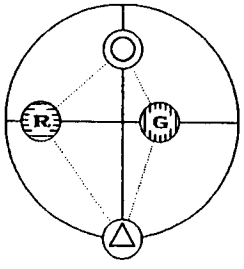

		INPUT	ΔOUT
COLOR	X1:	22	1.00
	X2:	20	7.00
FORM	Y1:	31	10.00
	Y2:	3	-10.00
MEAN:		21.00	
ΔMAX:		10.00	

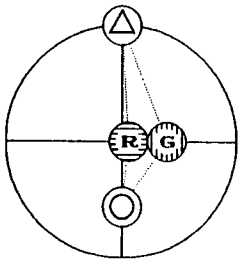

		INPUT	ΔOUT
COLOR	X1:	22	-6.00
	X2:	0	-20.00
FORM	Y1:	43	15.00
	Y2:	39	11.00
MEAN:		28.00	
ΔMAX:		20.00	

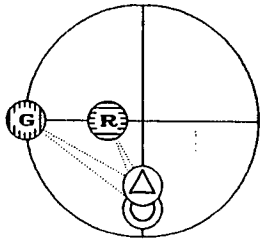

		INPUT	ΔOUT
COLOR	X1:	17	-15.75
	X2:	33	0.25
FORM	Y1:	37	4.25
	Y2:	44	11.25
MEAN:		32.75	
ΔMAX:		15.75	

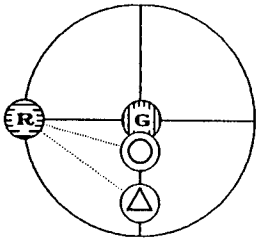

		INPUT	ΔOUT
COLOR	X1:	42	11.50
	X2:	14	-16.50
FORM	Y1:	17	-13.50
	Y2:	49	18.50
MEAN:		30.50	
ΔMAX:		18.50	

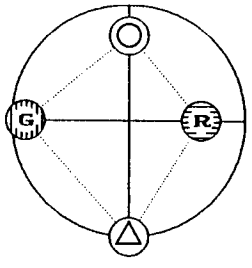

		INPUT	ΔOUT
COLOR	X1:	17	-10.50
	X2:	30	2.50
FORM	Y1:	39	11.50
	Y2:	24	-3.50
MEAN:		27.50	
ΔMAX:		11.50	

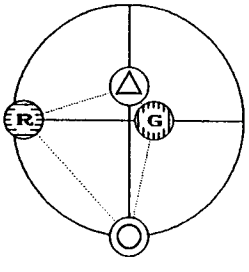

		INPUT	ΔOUT
COLOR	X1:	32	3.50
	X2:	46	17.50
FORM	Y1:	22	-6.50
	Y2:	14	-14.50
MEAN:		28.50	
ΔMAX:		17.50	

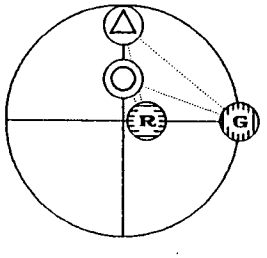

		INPUT	ΔOUT
COLOR	X1:	24	-2.00
	X2:	45	19.00
FORM	Y1:	5	-21.00
	Y2:	30	4.00
MEAN:		26.00	
ΔMAX:		21.00	

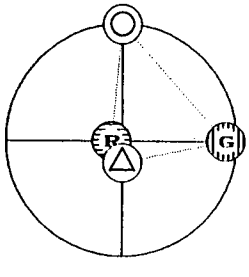

		INPUT	ΔOUT
COLOR	X1:	13	-12.00
	X2:	19	-6.00
FORM	Y1:	29	4.00
	Y2:	39	14.00
MEAN:		25.00	
ΔMAX:		14.00	

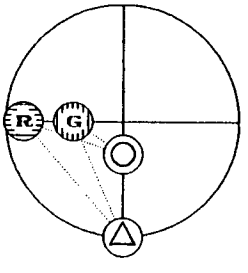

		INPUT	ΔOUT
COLOR	X1:	5	-2.50
	X2:	10	2.50
FORM	Y1:	5	-2.50
	Y2:	10	2.50
MEAN:		7.50	
ΔMAX:		2.50	

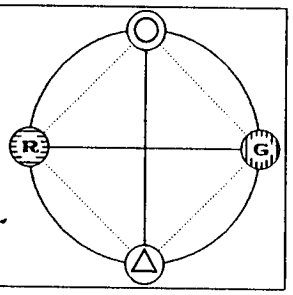

		INPUT	ΔOUT
COLOR	X1:	20	3.25
	X2:	6	-10.75
FORM	Y1:	37	20.25
	Y2:	4	-12.75
MEAN:		16.75	
ΔMAX:		20.25	

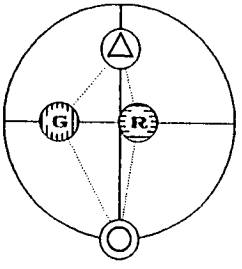

		INPUT	ΔOUT
COLOR	X1:	25	-10.00
	X2:	45	10.00
FORM	Y1:	43	8.00
	Y2:	27	-8.00
MEAN:		35.00	
ΔMAX:		10.00	

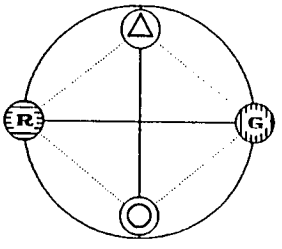

		INPUT	ΔOUT
COLOR	X1:	24	-2.75
	X2:	31	4.25
FORM	Y1:	34	7.25
	Y2:	18	-8.75
MEAN:		26.75	
ΔMAX:		8.75	

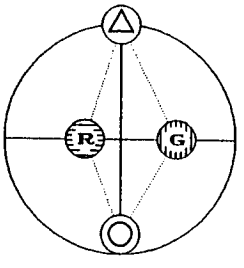

		INPUT	ΔOUT
COLOR	X1:	36	5.00
	X2:	37	6.00
FORM	Y1:	41	10.00
	Y2:	10	-21.00
MEAN:		31.00	
ΔMAX:		21.00	

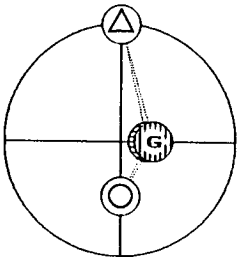

		INPUT	ΔOUT
COLOR	X1:	46	8.50
	X2:	31	-6.50
FORM	Y1:	43	5.50
	Y2:	30	-7.50
MEAN:		37.50	
ΔMAX:		8.50	

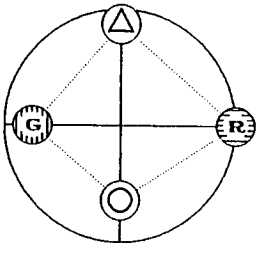

		INPUT	ΔOUT
COLOR	X1:	26	3.25
	X2:	7	-15.75
FORM	Y1:	49	26.25
	Y2:	9	-13.75
MEAN:		22.75	
ΔMAX:		26.25	

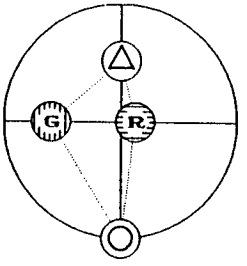

		INPUT	ΔOUT
COLOR	X1:	32	3.50
	X2:	46	17.50
FORM	Y1:	22	-6.50
	Y2:	14	-14.50
MEAN:		28.50	
ΔMAX:		17.50	

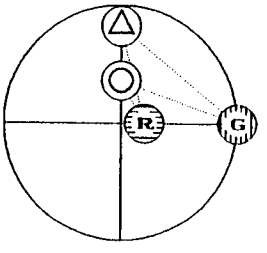

		INPUT	ΔOUT
COLOR	X1:	13	-12.00
	X2:	19	-6.00
FORM	Y1:	29	4.00
	Y2:	39	14.00
MEAN:		25.00	
ΔMAX:		14.00	

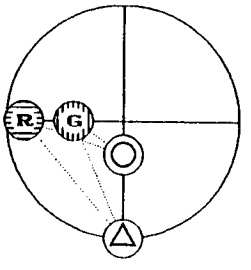

		INPUT	ΔOUT
COLOR	X1:	32	14.75
	X2:	6	-11.25
FORM	Y1:	23	5.75
	Y2:	8	-9.25
MEAN:		17.25	
ΔMAX:		14.75	

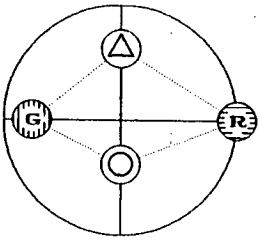

		INPUT	ΔOUT
COLOR	X1:	27	5.75
	X2:	12	-9.25
FORM	Y1:	22	0.75
	Y2:	24	2.75
MEAN:		21.25	
ΔMAX:		9.25	

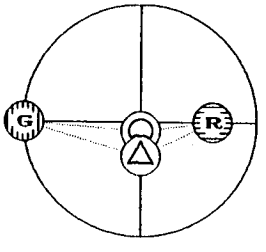

		INPUT	ΔOUT
COLOR	X1:	40	5.75
	X2:	18	-16.25
FORM	Y1:	29	-5.25
	Y2:	50	15.75
MEAN:		34.25	
ΔMAX:		16.25	

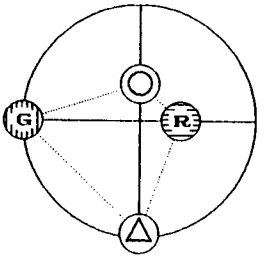

	INPUT	ΔOUT
COLOR X1:	5	-2.50
X2:	10	2.50
FORM Y1:	5	-2.50
Y2:	10	2.50
MEAN:	7.50	
ΔMAX:	2.50	

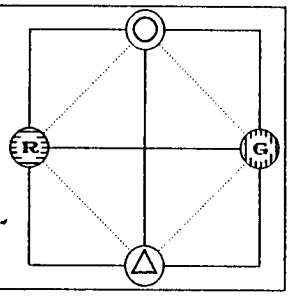

	INPUT	ΔOUT
COLOR X1:	22	1.00
X2:	28	7.00
FORM Y1:	31	10.00
Y2:	3	-18.00
MEAN:	21.00	
ΔMAX:	18.00	

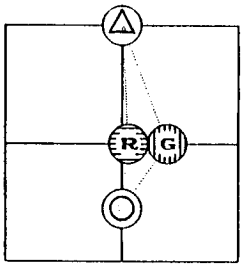

	INPUT	ΔOUT
COLOR X1:	22	-6.00
X2:	8	-20.00
FORM Y1:	43	15.00
Y2:	39	11.00
MEAN:	28.00	
ΔMAX:	20.00	

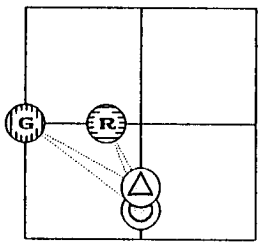

	INPUT	ΔOUT
COLOR X1:	7	-23.00
X2:	22	-8.00
FORM Y1:	42	12.00
Y2:	49	19.00
MEAN:	30.00	
ΔMAX:	23.00	

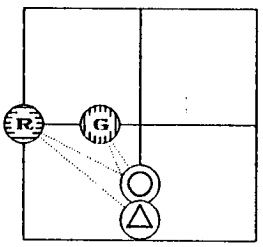

	INPUT	ΔOUT
COLOR X1:	42	11.50
X2:	14	-16.50
FORM Y1:	17	-13.50
Y2:	49	18.50
MEAN:	30.50	
ΔMAX:	18.50	

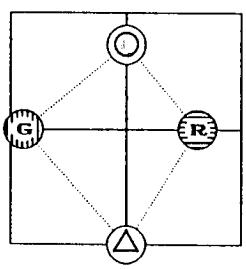

	INPUT	ΔOUT
COLOR X1:	26	3.25
X2:	7	-15.75
FORM Y1:	49	26.25
Y2:	9	-13.75
MEAN:	22.75	
ΔMAX:	26.25	

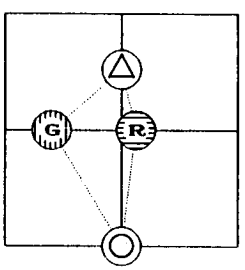

	INPUT	ΔOUT
COLOR X1:	28	3.25
X2:	6	-18.75
FORM Y1:	37	20.25
Y2:	4	-12.75
MEAN:	16.75	
ΔMAX:	20.25	

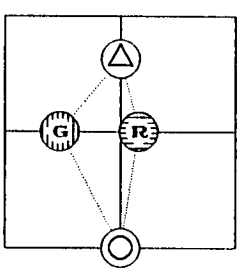

	INPUT	ΔOUT
COLOR X1:	32	3.50
X2:	46	17.50
FORM Y1:	22	-6.50
Y2:	14	-14.50
MEAN:	28.50	
ΔMAX:	17.50	

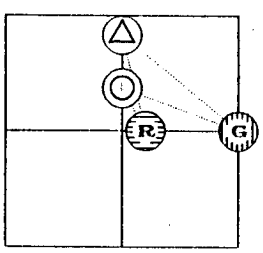

	INPUT	ΔOUT
COLOR X1:	25	-10.00
X2:	45	10.00
FORM Y1:	43	8.00
Y2:	27	-8.00
MEAN:	35.00	
ΔMAX:	10.00	

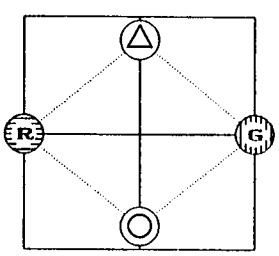

	INPUT	ΔOUT
COLOR X1:	13	-12.00
X2:	19	-6.00
FORM Y1:	29	4.00
Y2:	39	14.00
MEAN:	25.00	
ΔMAX:	14.00	

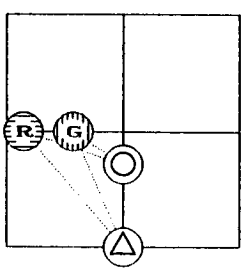

	INPUT	ΔOUT
COLOR X1:	24	-2.75
X2:	31	4.25
FORM Y1:	34	7.25
Y2:	18	-8.75
MEAN:	26.75	
ΔMAX:	8.75	

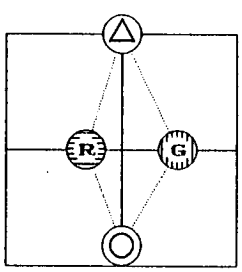

	INPUT	ΔOUT
COLOR X1:	28	-10.00
X2:	44	6.00
FORM Y1:	43	5.00
Y2:	37	-1.00
MEAN:	38.00	
ΔMAX:	10.00	

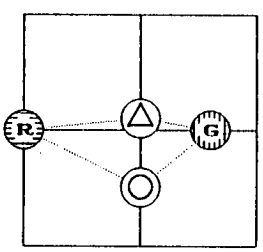

	INPUT	ΔOUT
COLOR X1:	5	-2.50
X2:	10	2.50
FORM Y1:	5	-2.50
Y2:	10	2.50
MEAN:	7.50	
ΔMAX:	2.50	

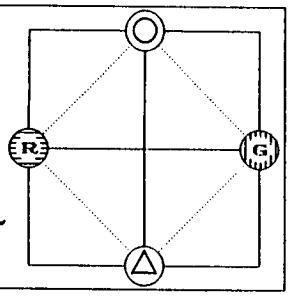

	INPUT	ΔOUT
COLOR X1:	47	19.25
X2:	44	16.25
FORM Y1:	2	-25.75
Y2:	10	-9.75
MEAN:	27.75	
ΔMAX:	25.75	

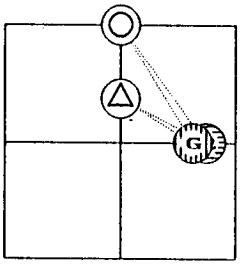

	INPUT	ΔOUT
COLOR X1:	50	10.50
X2:	42	2.50
FORM Y1:	35	-4.50
Y2:	31	-8.50
MEAN:	39.50	
ΔMAX:	10.50	

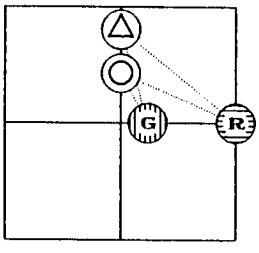

	INPUT	ΔOUT
COLOR X1:	40	31.25
X2:	2	-14.75
FORM Y1:	7	-9.75
Y2:	10	-6.75
MEAN:	16.75	
ΔMAX:	31.25	

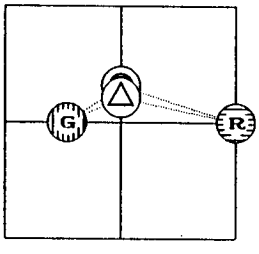

	INPUT	ΔOUT
COLOR X1:	1	-8.25
X2:	13	3.75
FORM Y1:	2	-7.25
Y2:	21	11.75
MEAN:	9.25	
ΔMAX:	11.75	

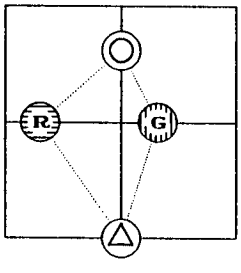

	INPUT	ΔOUT
COLOR X1:	22	-6.00
X2:	8	-20.00
FORM Y1:	43	15.00
Y2:	39	11.00
MEAN:	28.00	
ΔMAX:	20.00	

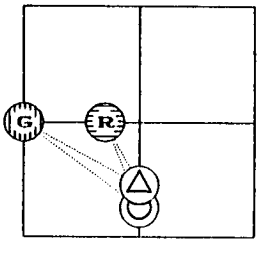

	INPUT	ΔOUT
COLOR X1:	39	21.50
X2:	4	-13.50
FORM Y1:	9	-8.50
Y2:	18	0.50
MEAN:	17.50	
ΔMAX:	21.50	

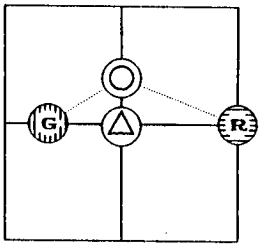

	INPUT	ΔOUT
COLOR X1:	10	-7.75
X2:	16	-1.75
FORM Y1:	6	-11.75
Y2:	39	21.25
MEAN:	17.75	
ΔMAX:	21.25	

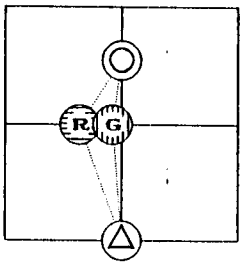

	INPUT	ΔOUT
COLOR X1:	20	4.75
X2:	16	-7.25
FORM Y1:	5	-18.25
Y2:	44	20.75
MEAN:	23.25	
ΔMAX:	20.75	

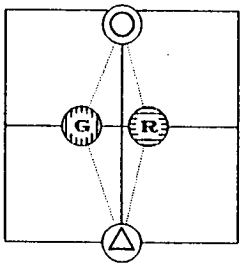

	INPUT	ΔOUT
COLOR X1:	5	-11.50
X2:	9	-7.50
FORM Y1:	22	5.50
Y2:	30	13.50
MEAN:	16.50	
ΔMAX:	13.50	

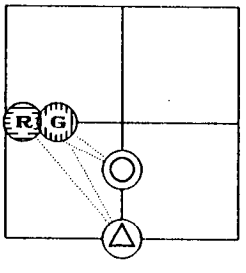

	INPUT	ΔOUT
COLOR X1:	22	1.00
X2:	28	7.00
FORM Y1:	31	10.00
Y2:	3	-18.00
MEAN:	21.00	
ΔMAX:	18.00	

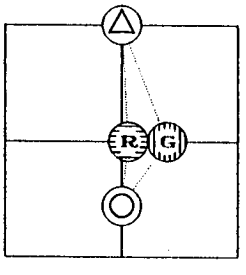

	INPUT	ΔOUT
COLOR X1:	17	-15.75
X2:	33	0.25
FORM Y1:	37	4.25
Y2:	44	11.25
MEAN:	32.75	
ΔMAX:	15.75